

The influence of the two-component grout on the behaviour of a segmental lining in tunnelling

*Original*

The influence of the two-component grout on the behaviour of a segmental lining in tunnelling / Oggeri, C., Oreste, P., Spagnoli, G.. - In: TUNNELLING AND UNDERGROUND SPACE TECHNOLOGY. - ISSN 0886-7798. - STAMPA. - 109:(2021). [10.1016/j.tust.2020.103750]

*Availability:*

This version is available at: 11583/2859154 since: 2021-01-14T22:58:05Z

*Publisher:*

Elsevier Ltd

*Published*

DOI:10.1016/j.tust.2020.103750

*Terms of use:*

This article is made available under terms and conditions as specified in the corresponding bibliographic description in the repository

*Publisher copyright*

(Article begins on next page)

1 **The influence of the two-component grout on the behaviour of a segmental lining in**  
2 **tunnelling**

3 Claudio Oggeri<sup>1</sup>, Pierpaolo Oreste<sup>2</sup>, Giovanni Spagnoli<sup>3</sup>

4 <sup>1</sup> Department of Environment, Land and Infrastructure Engineering, Politecnico di Torino,  
5 Corso Duca Degli Abruzzi 24, 10129 Torino, Italy, [claudio.oggeri@polito.it](mailto:claudio.oggeri@polito.it) ORCID 0000-  
6 0002-6848-8861

7 <sup>2</sup> Department of Environment, Land and Infrastructure Engineering, Politecnico di Torino,  
8 Corso Duca Degli Abruzzi 24, 10129 Torino, Italy, [pierpaolo.oreste@polito.it](mailto:pierpaolo.oreste@polito.it) ORCID:  
9 0000-0001-8227-9807

10 <sup>3</sup> **MBCC Group**, Dr-Albert-Frank-Strasse 32, 83308 Trostberg, Germany, Tel: +49 8621  
11 86-3702, [giovanni.spagnoli@mbcc-group.com](mailto:giovanni.spagnoli@mbcc-group.com) ORCID: 0000-0002-1866-4345

12 **Abstract**

13 Filling material is present around the segment lining when a shielded Tunnel Boring  
14 Machine is used to excavate a tunnel. The two-component grout is becoming lately one of  
15 the most used filling materials. Its mechanical properties evolve over time. Unfortunately,  
16 there are not many studies in the literature on the specific mechanical characteristics of  
17 these materials. This work presents the results obtained from an extensive laboratory test  
18 campaign that allowed to fully characterize the two-component filling material during the  
19 setting period. In particular, the values of the stiffness and resistance parameters were  
20 obtained over time, where uniaxial compression tests and oedometer tests were carried  
21 out. A detailed study of the effect of the presence of the filling material on the behavior of  
22 the support system (segmental lining + filling material) was developed for two of the most  
23 widespread analytical methods for the analysis of the behavior of tunnels and structures of

24 support: the convergence-confinement method and the Einstein and Schwartz method.  
25 Subsequent parametric analyses made it possible to consider the variability of the  
26 influencing parameters within the typical variability ranges obtained from the laboratory  
27 test campaign or known from the available scientific literature. From the study carried out,  
28 it was possible to note that it is necessary to consider the presence of the filling material in  
29 the evaluation of the stiffness of the support system, when using the convergence-  
30 confinement method to estimate the loads acting on segmental lining. In this regard, it is  
31 necessary to have a reliable estimate of the elastic modulus of the filling material in the  
32 period of loading of the segmental lining. On the other hand, the presence of the ring of  
33 filling material is negligible when evaluating the state of stress of the segmental lining with  
34 specific methods capable of considering the rock-support interaction. In particular,  
35 adopting the Einstein and Schwartz method, it is possible to define the bending moments  
36 and normal forces acting in the support structure, referring to the stiffness parameters of  
37 the segmental lining alone.

38 **Key words:** two-component grout; curing time; oedometer; unconfined compressive  
39 strength; TBM; convergence-confinement method; Einstein and Schwartz method.

40

41 **Abbreviations and nomenclature**

- 42  $A_s$  Area of the cross section of the support, through a plane passing through the axis of  
43 the tunnel;
- 44  $b_s$  Width of the support section in the direction of the tunnel axis, considered equal to 1  
45 m;
- 46  $c$  Cohesion of the rock mass;
- 47  $C^*$  Compressibility ratio of the support;
- 48  $E$  Elastic modulus of the rock mass
- 49  $E_{fm}$  Elastic modulus of the filling material;
- 50  $E_{s,eq}$  Equivalent elastic modulus of the support;
- 51  $E_{sl}$  Elastic modulus of the segmental lining concrete;
- 52  $F^*$  Flexibility ratio of the support;
- 53  $I_s$  Moment of inertia of the cross section of the support, through a plane passing  
54 through the axis of the tunnel;
- 55  $K_0$  Lateral earth coefficient at rest;
- 56  $k_{sys}$  Reaction line of the support the stiffness;
- 57  $M_{max}$  Maximum bending moment present in the lining;
- 58  $N$  Normal force present in the lining;
- 59  $p$  Pressure inside the tunnel acting on the walls;
- 60  $p_{eq}$  Final entity of the loads acting on the support structure;

61	$p_0$	Hydrostatic initial stress state (undisturbed);
62	$R$	Tunnel radius;
63	$R_{pl}$	Plastic radius of the tunnel;
64	$t_{s,eq}$	Thickness of equivalent support;
65	$t_{fm}$	Thickness of the filling material;
66	$t_{sl}$	Thickness of the segmental lining;
67	$u_{eq}$	Final displacement of the tunnel wall in the radial direction;
68	$u_{max}$	Maximum displacement of the tunnel wall in the absence of supports;
69	$u_0$	Displacement of the tunnel wall when the support structure is installed;
70	$u_R$	Radial displacement of the tunnel wall;
71	$\nu$	Poisson ratio of the rock mass;
72	$\nu_{fm}$	Poisson's ratio of the filling material;
73	$\nu_{sl}$	Poisson's ratio of the concrete constituting the segmental lining;
74	$\alpha_f$	Angle of the failure plane;
75	$\varphi$	Friction angle of the rock mass;
76	$\Psi$	Dilatancy of the rock mass;
77	$\sigma_r$	Radial stress in the point where the stress state is evaluated during the design of
78		the support structure;
79	$\sigma_{vert}$ or $\sigma_v$	Vertical load during the oedometer tests;
80	$\sigma_{\theta,sl,in}$	Circumferential stress at the intrados of the segmental lining due to moment;

81  $\sigma_{\theta, fm, ex}$  Maximum circumferential load on the extrados of the filling material due to  
82 the moment;

83  $\sigma_{\theta, sl}$  Constant load in the segmental lining section due to the nominal force;

84  $\sigma_{\theta, fm}$  Constant load in the section of the filling material due to the nominal force;

85  $\xi$  Incremental coefficient taking into into account the transfer of stresses from one ring  
86 to the adjacent one, in correspondence with the longitudinal joints of the segmental lining;

87  $\eta$  Reduction coefficient taking into account the presence of longitudinal joints in  
88 segmental lining;

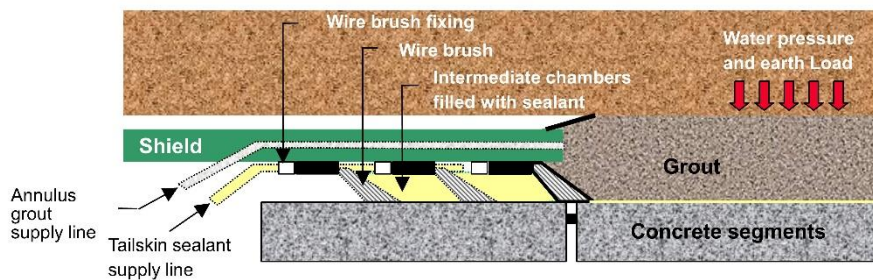
89  $\phi'$  Slope the Mohr Coulomb envelope.

90

91

92        **1. Introduction**

93        During the excavation with shielded tunnel boring machines (S-TBM) pre-cast segments  
94        are commonly installed as tunnel lining and for support purpose. Due to overcutting of the  
95        circular tunnel profile due to the TBM cutterhead excavation, a circular gap between the  
96        lining and the surrounding ground is formed (thickness about 13 to 20 cm, e.g. Talmon and  
97        Bezuijen, 2005; Beghoul and Demagh, 2019). This space must be filled by pumping or  
98        injecting some materials, such as the so-called “annulus grout” (Fig. 1). The practical aims  
99        for the use of the filler are linked to control the ground deformation around the lining gap  
100        and the reduction of the ground loss; there is also a role to contribute in a regular and  
101        homogeneous distribution of the contact pressure at the interfaces ground/grout and  
102        grout/segmental lining.



103

104        **Fig. 1. Sketch of the annulus grout.**

105

106        There are two basic types of annular grouts currently in use: thick mortar type grouts and  
107        highly mobile two-component grouts. The typical mix-design in a m<sup>3</sup> system for a two-  
108        component grout is very variable and depends strongly on the project specification but in  
109        general it consists of cement (280-450 kg), bentonite (30-60 kg), water (730-860 kg),  
110        retarder 3-5 kg) and accelerator, normally sodium silicate (60-80 kg).

111        The accelerator (“B” component) is generally added just before pumping phase of the mix  
112        of water, bentonite, retarder and cement (“A” component).

113 The excavation of the tunnel produces a relaxation of the initial tensional state, leading to  
114 deformations in the ground from certain distance ahead of the excavation face. The  
115 convergence in the tunnel is the inward displacements of the soil/rock as consequence of  
116 the relief of the initial stress. In case of no support, the ground is free to deform into the  
117 cavity until arriving to the equilibrium state.

118 The role of the two-component grout is very important for the correct mechanized  
119 tunneling procedure in order to minimize surface settlements due to any over-excavation  
120 generated by the passage of the TBM (e.g. Maidl et al., 1995) or to minimize the loads  
121 acting on the segmental lining, although grouting can also be used for the same aims (e.g.  
122 Komiya et al., 2001). The two-component grout should be water-tight, be pumpable, be  
123 workable, able to fill the void, not able to shrink, to stiff quickly and to be wash-out resistant  
124 (e.g. Thewes and Budach, 2009). Its mechanical strength, though, should be only slightly  
125 higher than that of the surrounding soil to prevent substantial normal force components  
126 being removed from the annular gap mortar in the final state (DAUB, 2013). Simultaneous  
127 backfilling with two-component grouts, in comparison with the mortar type grouts, keeps in  
128 general lower settlements during TBM excavation (Hirata, 1989) and normally the lining  
129 pressures, few rings behind the TBM, do not change significantly in the long-term  
130 (Hashimoto et al., 2004).

131 However, not many works dealt with the behavior of the two-component grouts both  
132 experimentally and numerically (e.g. Pelizza et al., 2011; Shah et al., 2018; Ochmański et  
133 al., 2018; Todaro et al., 2019). For instance, it is well-known that the mechanical properties  
134 of the two-component grout change based on the mix-design type (Flores, 2015; Todaro et  
135 al., 2019). Besides, tail void grouting, as it cannot be directly observed after the tunnel  
136 construction, is difficult to simulate (Dai et al., 2010). Oh and Ziegler (2014), Shah et al.  
137 (2018), Ochmański et al. (2018) more recently Ochmański et al. (2020) performed a

138 numerical analysis regarding the effects of the two-component grout on the tunnel  
139 settlement. Bezuijen and Talmon (2003) and Dias and Bezuijen (2015) investigated the  
140 consolidation of the grout, which seems to be dependent on the permeability of the  
141 surrounding soil as the latter determines the rate of outflow. Therefore, a very  
142 impermeable soil like a clay could stop the grout from consolidating (Vu et al. 2016),  
143 however in permeable soils, fluid loss occurs during grout consolidation (Talmon and  
144 Bezuijen, 2005). Furthermore, Bezuijen and Talmon (2003) and Dias and Bezuijen (2015)  
145 illustrate that during this consolidation, the grout mixture becomes thicker (the cement-  
146 water ratio increases, decreasing the viscosity of the mixture). Talmon and Bezuijen  
147 (2005) investigated the stress-strain modelling of the grout.

148 However, the role of the material considering the deformability and resistance values that  
149 characterize it during the loading phase of the segmental lining tunnel are not fully  
150 investigated. The two-component grout when hardens should transmit the tunnel  
151 deformation to the ground. In literature, ground settlement in tunneling caused by ground  
152 loss (i.e. the difference between actual and theoretical excavation volume) considers also  
153 tail loss which occurs along the annular void between ground and concrete segmental  
154 lining (as a result of shrinkage or compression of backfill grout material). The gap model  
155 proposed by Lee et al. (1992) is based on simple elastic equations for the squeezing of  
156 tunnel face and the contraction of excavated cavity and it has some limitations and  
157 uncertainties for practical use (Park et al., 2018). Finally, features of specific products and  
158 fulfillment of requirements should be addressed when adopting design criteria and  
159 accepting construction procedures: materials, environmental requirements and use of  
160 chemicals products should be approved by Client and Boards for a reliable practical quality  
161 assurance (Oggeri and Ova, 2004). Furthermore, the use of numerical modeling in  
162 tunneling, both with two-dimensional and three-dimensional methods, requires the  
163 definition of the characteristics of all the materials that are used as support structures or

164 rock reinforcement interventions (Do et al., 2014a; 2014b; 2015; 2016; Pelizza et al.,  
165 2000).

166 In this paper, a mix-design of a two-component grout was analyzed in the detail.  
167 Unconfined compressive strength (UCS) and oedometer tests at varying curing ages were  
168 investigated. From the analysis of the laboratory results it was possible to detect the  
169 behavior of this material and in particular the deformability and strength values that  
170 characterize it during the loading phase of the segmental lining tunnel.

171 Two very interesting simplified approaches are available in the literature to study the  
172 behavior of the supporting structures in tunnelling: the convergence-confinement method  
173 (e.g. Oreste, 2007; Oreste et al., 2016; 2018a; 2018b; Spagnoli et al., 2016; 2017) and the  
174 method of Einstein and Schwartz (1979). **The convergence-confinement method considers**  
175 **the ground response to the advancing tunnel face and the interaction with installed support**  
176 **(e.g. Oke et al. 2018), whereas the latter method assumes an annular support**  
177 **continuously connected with the wall of a deep and circular tunnel.**

178 This article describes the techniques for correctly considering the presence of the filling  
179 material in the gap between the tunnel segmental lining and the tunnel wall using the two  
180 widespread simplified analysis methods listed above. Some calculation examples will allow  
181 to evaluate the effect of the filling material on the static behavior of the tunnel segmental  
182 lining, starting from the mechanical parameters evaluated by the extensive laboratory  
183 testing campaign. From the developed analyses it will be possible to obtain useful  
184 information on how to consider the presence of the filling material ring in the design phase  
185 of the segmental lining of a tunnel.

## 186 **2. The mechanical behavior of the two-component grout in the laboratory**

### 187 Testing procedures

188 The following mix-design was tested during this experimental campaign: water 800 g,  
189 bentonite 35 g, cement (CEM I 52.5) 350 g, retarder 17.5 g (solution contains 20% solid  
190 therefore retarder dosage by weight of cement is 1%) and water glass (sodium silicate) 85  
191 g (water glass is the “B” component so it is about 7% weight of the mix represented by the  
192 component “A”). Based on the grout component quantities, a preliminary laboratory testing  
193 set has been carried out. The purpose of such a trial was to identify the basic mechanical  
194 properties of the grout at different duration of the curing and to observe the failure modes  
195 as well. Following the experimental raw data on compressive strength, deformability and  
196 unit weight have been processed in order to be adopted in the mathematical modelling for  
197 interaction and also for general description of the mechanical behaviour.

198 Preparation of fluid grout has been carried out with bentonite slurry hydration (duration at  
199 least 24 h) and subsequent mixing with retarder, cement and waterglass catalyst, by  
200 respecting the mass percentages provided for the standard mix. Both a manual dispersion  
201 and a high-speed rotating mixer (up to 8000 rpm) have been adopted during this phase.  
202 Weight has been determined by means of 0.01 g precision scale.

203 Sample preparation has been carried out by using specimen casing where the catalyst has  
204 been added to fluid grout and fast rotation of mixer has allowed to disperse and  
205 homogenize the grout. Then the casing has been recovered in a box for curing in water.  
206 Curing procedure has been selected the following timeline for testing: 1 hour; 24 hours; 7  
207 days; 28 days.

208 Preparation of specimen requires great care and repeated attempts are necessary to  
209 obtain suitable material. This is due to the great sensitivity of final features of the specimen  
210 to addition and mixing of water glass. This step has been made with the mentioned high  
211 speed mixer in order to be sure that dispersion of water glass is homogeneous and quick  
212 inside the grout when still fluid.

213 Grout (without component “B”) viscosity testing with Marsh cone carried out by using a  
214 funnel as described in the API Recommended Practice 13B-1 (2014) produced a result  
215 between 30 and 45 seconds. Bleeding of the grout (without component “B”) according to  
216 the DIN EN 480-4 (2006) was less than 3% at 3 hours. Final mixing of components “A”  
217 and “B” produced a total gel time of less than 9 seconds.

218 Uniaxial compression testing has been carried out in a Belladonna mechanical press for  
219 soils, equipped with bidirectional displacement rate control device (Fig. 2). Transducers  
220 used to measure load and displacements have been respectively a full bridge load cell  
221 (CCT model, full scale 5 kN and precision of 1 N) and LVDT devices (HBM models,  
222 precision 0.001 mm). Vertical displacement has been measured following the relative  
223 movement of the base of the specimen and radial displacements have been measured by  
224 using two transducers mounted on opposite and diametral alignment across the specimen.  
225 An alternative solution for displacement measurement has not been possible. As the  
226 external surface of specimen was not showing adhesive properties and due to the short  
227 timeline available between preparation and testing for the majority of specimen, strain  
228 gages have not been glued onto the specimen. Radial LVDT transducers have been  
229 mounted to be in contact within the medium third of the specimen height.

230 Advancing rate has been adapted in the range of 0.15÷0.45 mm/min and the suitable  
231 results have been obtained for the range 0.30÷0.45 mm/min; this selection is a good  
232 compromise to avoid creep behavior (excess of lateral swelling) or sudden failure (vertical  
233 cracks). Specimen diameter has been selected at 48 mm; for one additional sample the  
234 diameter was 52 mm and for two large diameter specimens the value was 75 mm.

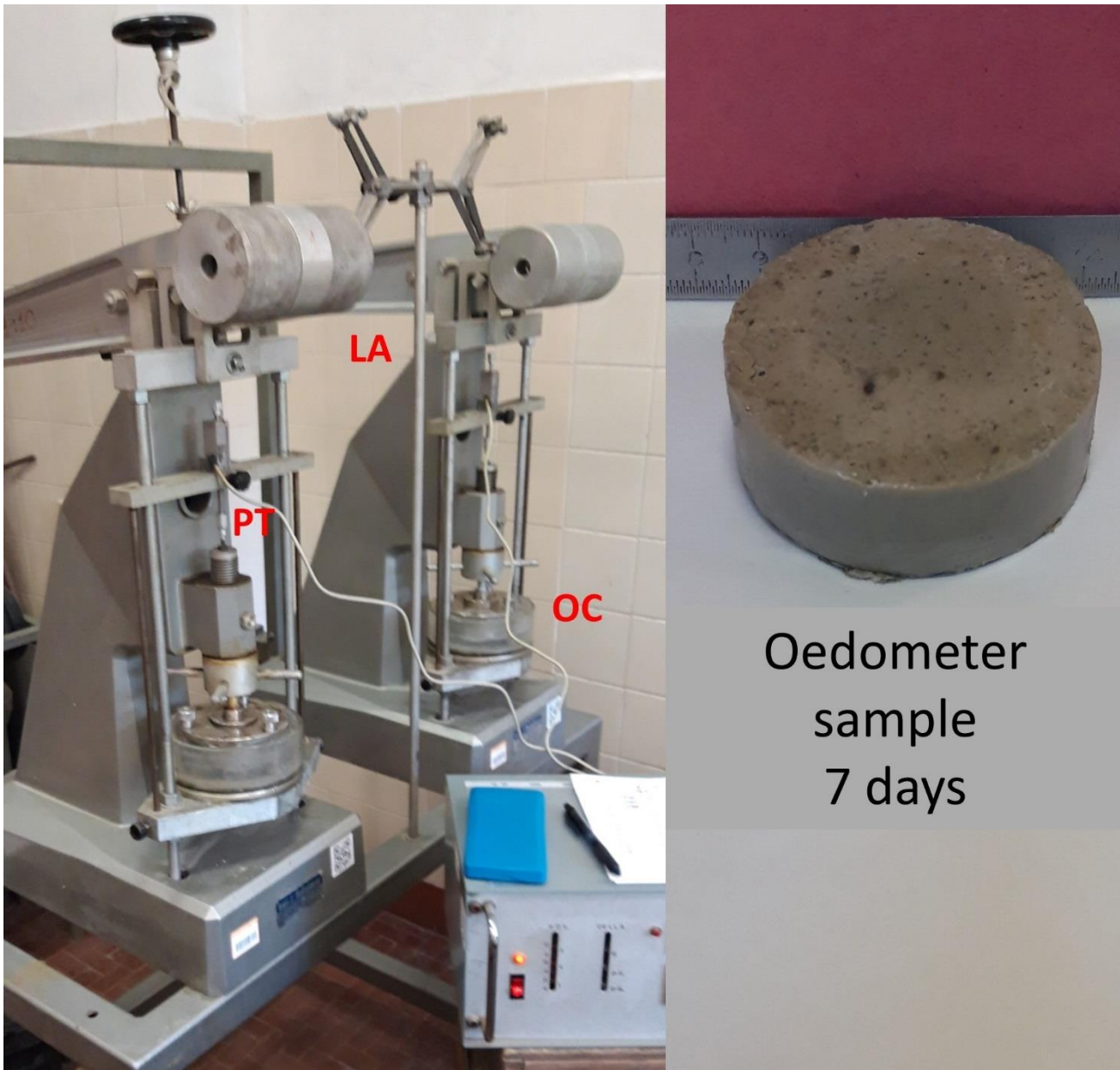


235

236 **Fig. 2 Testing equipment for compression (left) and enlargement of the UCS sample**  
 237 **(right). LC: load cell; GS: grout sample; LVDT: radial coupled LVDT transducers;**  
 238 **vLVDT: vertical LVDT transducer; PB: base of press plate; RCD: device for advance**  
 239 **rate control.**

240 Oedometer testing has been performed by using a standard mechanical oedometer  
 241 Belladonna equipment (Fig. 3). Ring type has been selected with net diameter of 50 mm  
 242 and height of 20 mm; this size is sufficient to respect grain size distribution of formed  
 243 grout. The standard test methods for one-dimensional consolidation properties of soils  
 244 using incremental loading have been adapted to respect the fact that grout is curing during  
 245 testing, and thus a compromise was necessary to avoid long term duration typical of  
 246 oedometer tests in soils (from days to weeks for and an entire loading-unloading cycle).

247 Specimens have been maintained saturated during cycles, and displacement have been  
248 measured by means of potentiometric transducers with precision of 0.01 mm.



249

250 **Fig. 3. Twin Bishop oedometer equipment used for grout testing (left) and**  
251 **oedometer two-component grout sample (right). LA: loading arm; OC: oedometer**  
252 **cell with specimen; PT: potentiometric transducer for vertical settlement.**

253 Additional testing has been devoted to obtaining some auxiliary information with the  
254 determination of apparent unit weight (geometrical determination, so **unit weight has been**  
255 **determined with the geometrical measurement of the volume of specimen casing and of**

256 the weight of ingredients used to fill that volume) and surface strength (by means of soil  
257 pocket penetrometer).

258

## 259 Laboratory test results

### 260 *Compression test results*

261 The main results after uniaxial compression testing are reported in Tab. 1. Strength is  
262 considered as the maximum value of stress obtained, for the great majority of cases, at  
263 yield at the end of the elastic domain. Deformability values are indexed as secant moduli  
264 and Poisson coefficient at 25%, 50% and 75% of the elastic domain and as tangential  
265 values at 50% of the elastic domain.

266

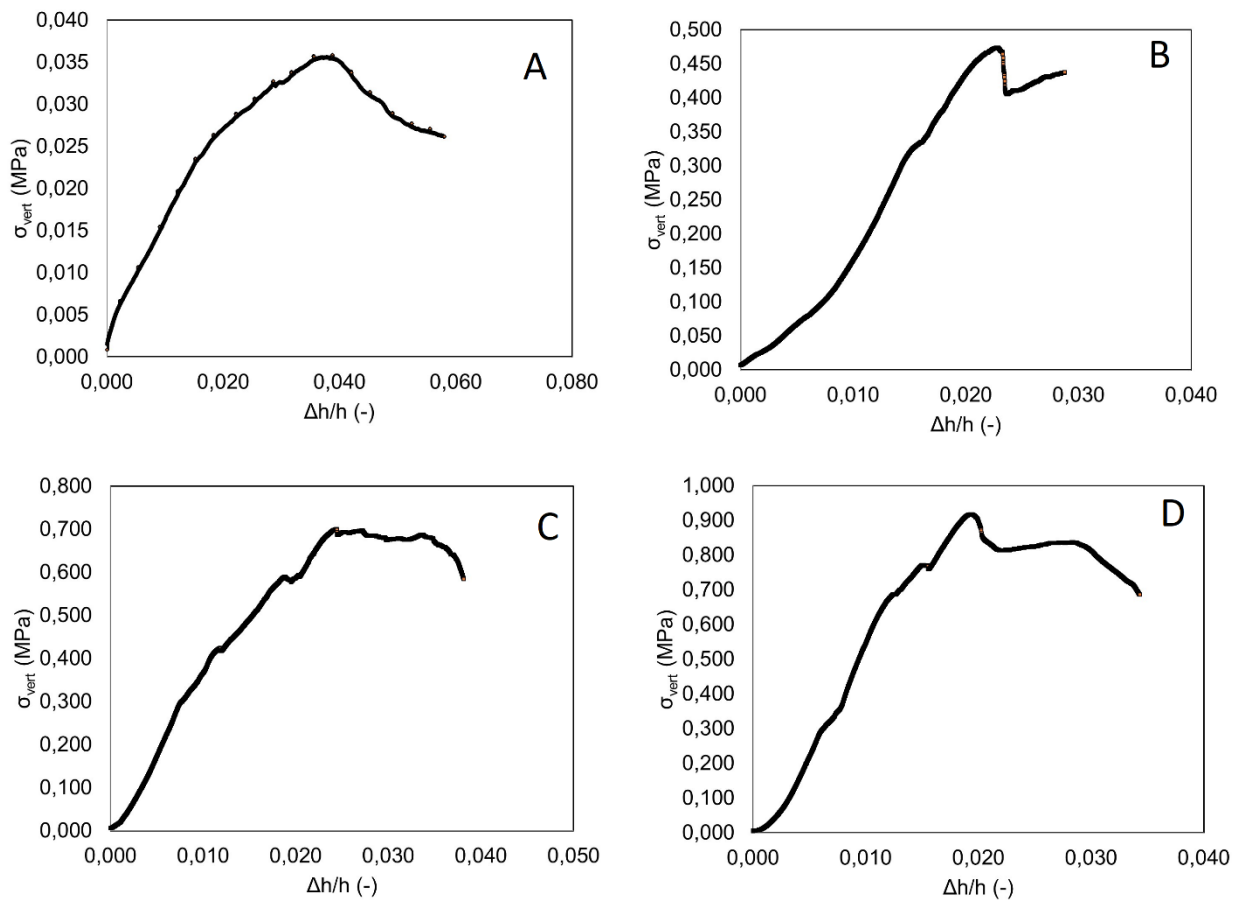


n.1	1.240	0.92	44.4	52.0	55.2	76.7	0.03	0.03	0.04	0.06
n.2	1.233	0.40	10.6	16.9	19.0	34.5	0.15	0.14	0.11	0.12
n.3	1.239	0.84	29.2	37.8	47.7	77.5	0.14	0.10	0.08	0.04
n.4	1.143	0.50	27.6	38.1	39.8	68.6	0.03	0.03	0.05	0.03

268 **Table 1. Results obtained for the two-component grout at different curing timelines in uniaxial condition of compression.**  
269 **Diameter of specimen is usually 48 mm if not indicated. The pedix “s” means secant value, the pedix “t” means tangent**  
270 **value, the pedix “fm” means filling material, UCS: uniaxial compressive strength. Mix components are in the same proportion**  
271 **for the specimen as referred in chapter 2.**

272

273 In Fig. 4 there is a representative sequence of vertical stress – vertical strain curves at  
274 different curing timelines.



275

276 **Fig. 4. Vertical stress - strain curves at different curing timelines for the grout. (A)**  
277 **curing time 1 hour, (B) curing time 24 hours, (C) curing time 7 days and (D) curing**  
278 **time 28 days. Each x and y-axis have different scale, adapted for each graph in**  
279 **order to properly show the curve shape. Legend:  $\sigma_{vert}$ : vertical stress;  $\Delta h/h$ : vertical**  
280 **strain, ratio of the vertical displacement on the sample height.**

281 **The observed UCS values are rated slightly lower than expected due to the higher amount**  
282 **of retarder introduced. This was intentional, in order to asses also the particular effect of**  
283 **retarder, even if this is not linked to a specific mix design necessarily adopted in practice.**

284 Testing in compression has generally been regular and vertical stress vs. vertical strain is  
285 reliable both in the elastic and in the post peak field. A clear yielding and softening  
286 behaviour has been observed, with some subvertical and inclined cracks prevailing. In  
287 some cases, a pseudoconical shape at failure has been found at the extremities of the  
288 specimen, thus respecting the ideal Mohr-Coulomb criterion failure geometry (Fig. 5). The  
289 grain size of the cured grout specimens considered as valid appears regular and  
290 homogeneous, without veins or lenses at different consistency.

291 The adoption of a linear Mohr – Coulomb criterion allows one to establish a relationship  
292 between the angle of the failure plane  $\alpha_f$  and the slope  $\phi'$  of the Mohr Coulomb envelope.

293 The failure angle measured relative to the plane of the major principal stress is:

$$294 \quad \alpha_f = 45^\circ + \frac{\phi'}{2} \quad (1)$$

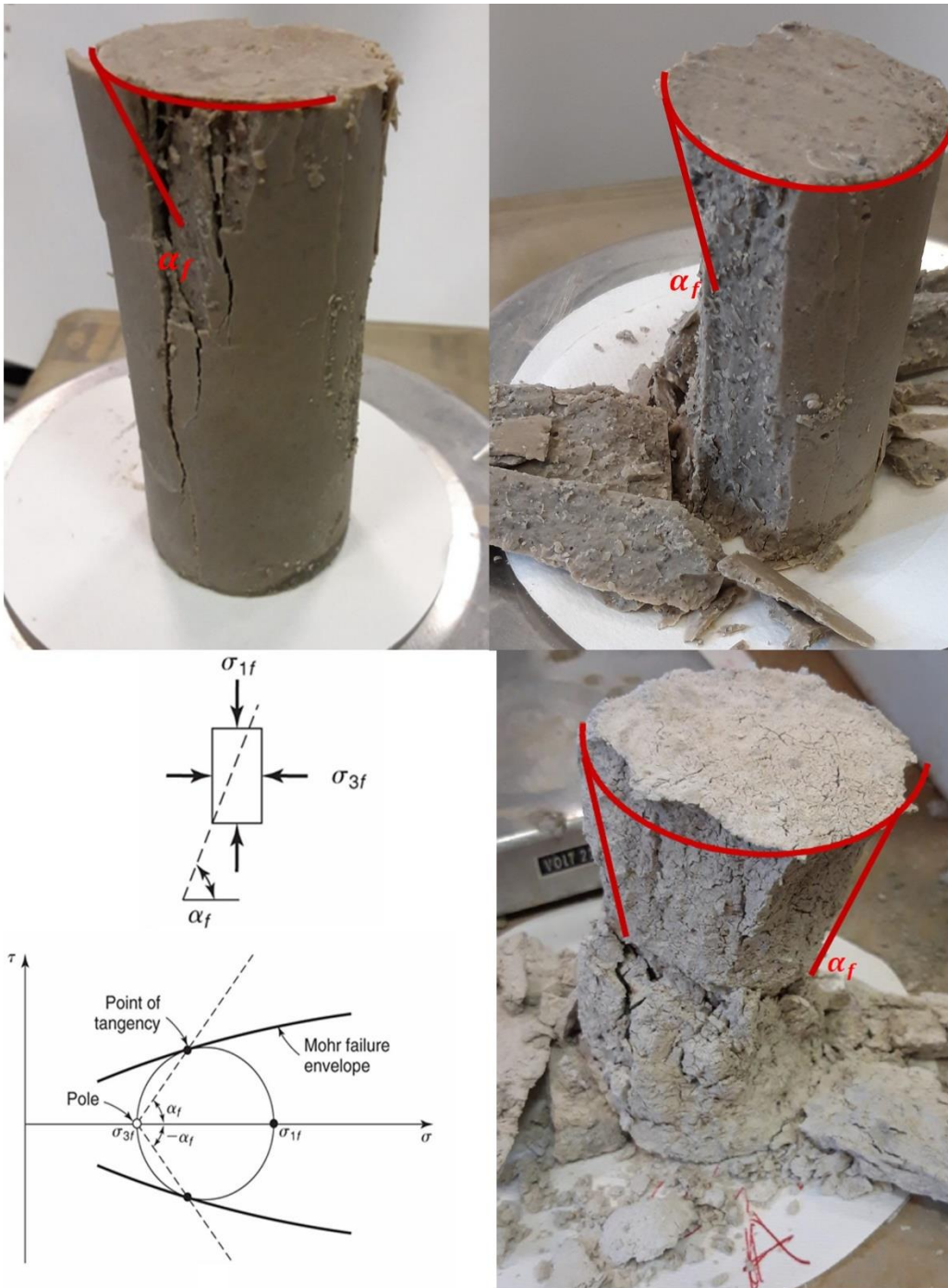
295 In case of UCS of a cohesive material, it is possible also to set:

$$296 \quad UCS = \frac{2*c'*\cos\phi'}{1-\sin\phi'} \quad (2)$$

297 The evidence that some of the failed specimens have exhibited a quite defined angle of  
298 the failure planes can lead to an estimation of the friction angle and also of the cohesion of  
299 the grout.

300 In Fig. 5 some examples of measured angles at failure are shown; it is necessary to  
301 outline that this behaviour has not been clearly observed at the shorter curing time (1 h),  
302 probably due to the wide peak and softening of the stress – strain curve in compression  
303 that is linked to the distribution of growing cracks of the fresh grout. Easier to be observed  
304 at longer curing timelines, where the linear part of the stress–strain curve allows to  
305 maintain more defined and extended cracks. Common measured values of  $\alpha_f$  are inside  
306 the range of  $65^\circ \div 68$ , corresponding to values of  $\phi'$  of about  $40^\circ \div 46^\circ$ . Due to the relatively  
307 small number of tested specimens, it is not still possible to establish a trend of the friction

308 angle depending on the curing time. It is necessary to outline that shear strength  
309 parameters are also depending on the water/cement ratio, on the amount of water glass  
310 catalyst and on the percentage of bentonite, clearly variable for each grout mixing type and  
311 thus affecting the evolution of such parameters with curing. The raw correspondence  
312 among the involved parameters  $\alpha_f$ ,  $\phi'$ , UCS, and  $c'$ , according to the available data,  
313 provides values of  $c'$  in the following ranges: after 24hours: 85÷95 kPa; after 7 days:  
314 90÷100 kPa; after 28 days: 135÷155 kPa.



315

316 **Fig.5. Some specimens after failure: on the upper ends the typical conical shape is**  
 317 **developed and lateral slabbing as well, due to fine and homogenous grain size of**  
 318 **the grout. The “A” specimen (bottom-right picture) has a diameter of 75 mm and it is**  
 319 **desiccated. The graphical scheme of the specimen is showing the position of the**  
 320 **failure plane and the corresponding link with the Mohr failure envelope.**

321 Figure 6 shows a representative specimen during the compression test and at failure at 28  
322 days curing time. Failure appears as progressive, with slabbing and inclined cracking  
323 propagation.



324

325 **Fig. 6. Sequence of loading and failure after 28 days curing of the grout.**

326 Less easy to be interpreted is the radial strain, at least for two reasons: the first is the  
327 possibility to locate the LVDT in the zone of growing microcracks, that can both push out  
328 the transducers or to leave them to move inside the crack opening; the second is that, in  
329 any case, the greater and compulsory behaviour is clearly following the closure of  
330 micropores and damage of cemented structure of the grout, and this happens along the

331 vertical direction. Concerning the possible evolution of strength parameters, observation  
332 are still provisional due to the limited number of tested specimen that cannot allow one to  
333 be so confident with characteristic values of strength parameters; preliminary results  
334 seems that the greater effect will be on cohesion rather than in friction angle.

335

### 336 Oedometer test results

337 Confined compression tests can provide essential data in order to understand the behavior  
338 of the grout mix, at different curing timelines and at different levels of vertical stress. The  
339 fine-grained grout has allowed to use the 50 mm ring diameter as considered to be  
340 representative for the geometrical scale of the material. Curing and testing have been  
341 carried out in saturated conditions.

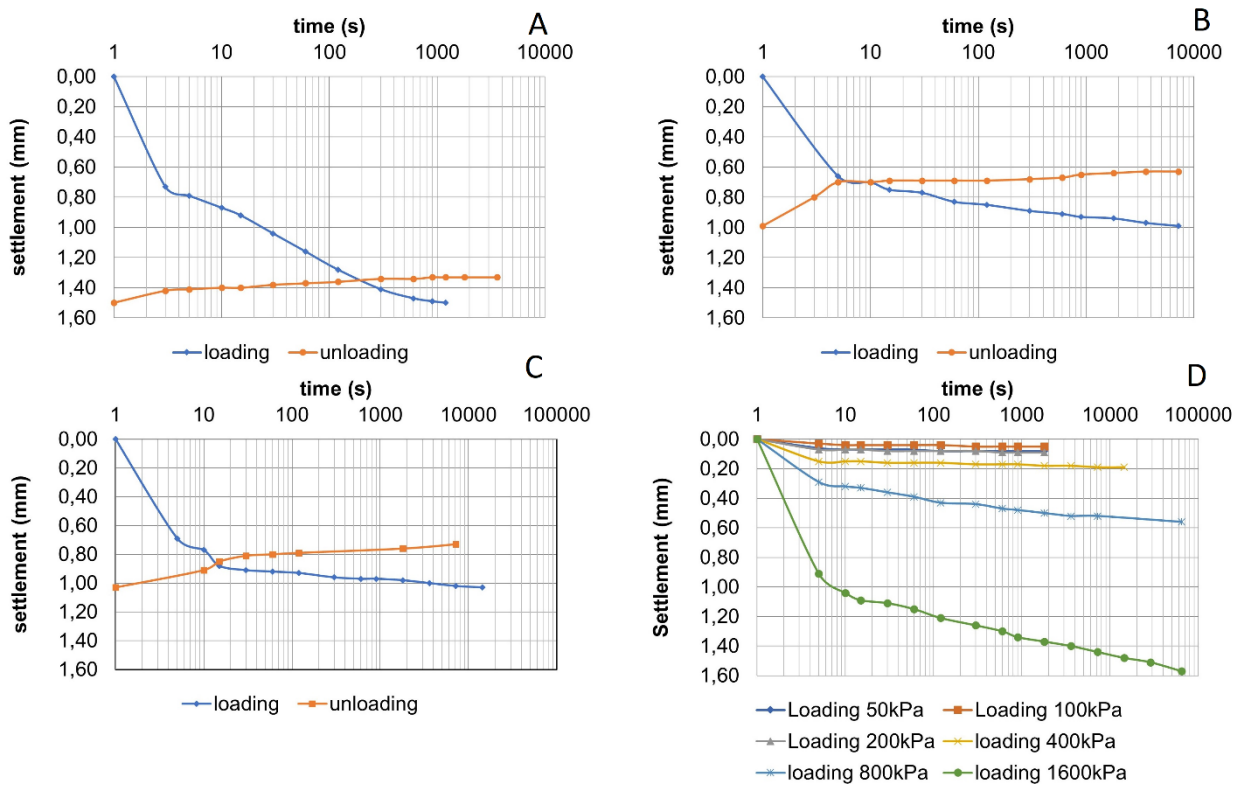
342 During this testing session four curing timelines have been adopted and loading –  
343 unloading cycles have been carried out, namely following the following scheme:

- 344 • curing 1 hour: 6 new specimens, each of them loaded and unloaded at the  
345 respective vertical stress of 50, 100, 200, 400, 800 and 1600 kPa; loading phase  
346 has been extended for about 20 minutes, in order to respect the corresponding  
347 duration of curing; unloading phase has been driven directly by removing the total  
348 applied load for another 20 minutes;
- 349 • curing 24 hours: 6 new specimens with the same procedure just described, apart for  
350 the duration of loading and unloading phases, which have been extended to 2  
351 hours;
- 352 • curing 7 days: 2 new specimens, both loaded at 400 kPa for 6 hours for  
353 comparison; then the load on the first specimen has been raised to 1200 kPa for  
354 another 4 hours and finally unloaded to zero by measuring displacements for a time

355 lapse of 2 hours; the second specimen after loading at 400 kPa has been unloaded  
356 to zero in a time lapse of 2 hours;

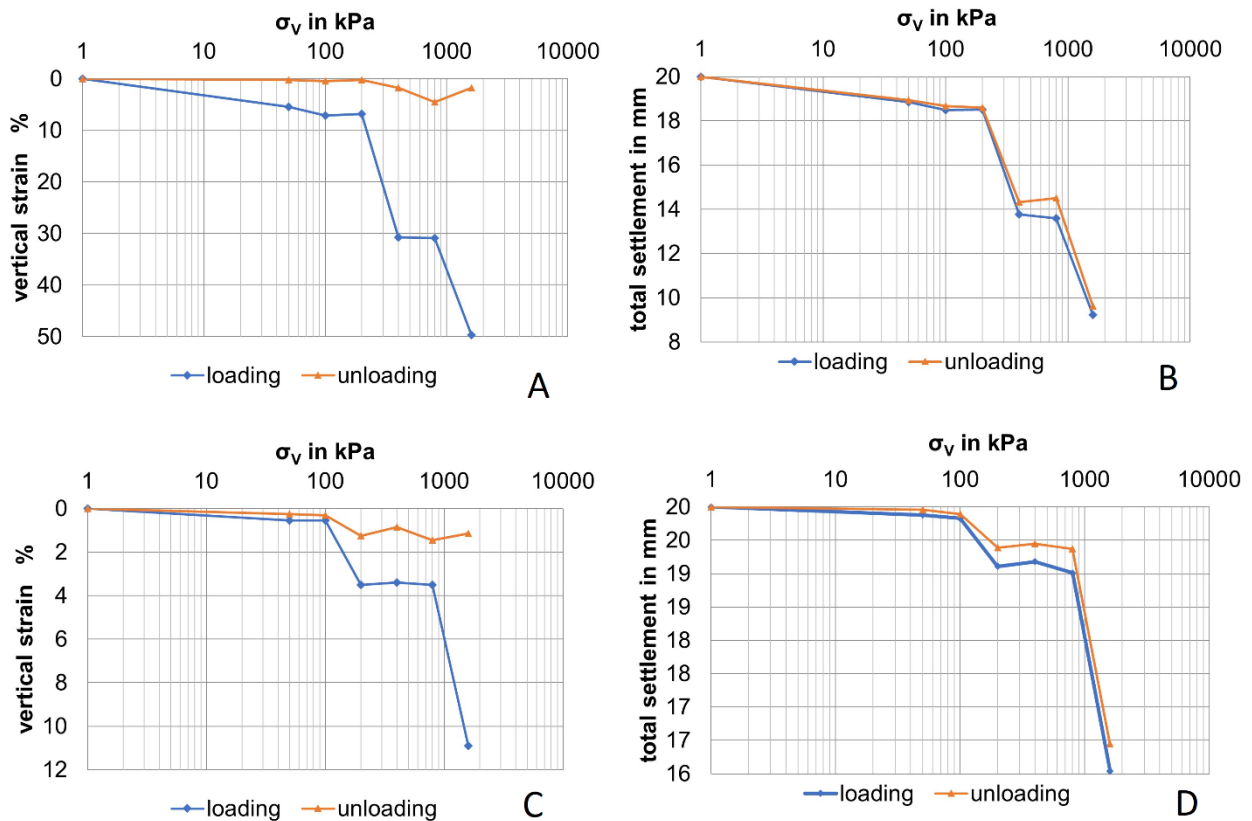
357 • curing 28 days: 2 new specimens, for comparison, each of them step loaded at the  
358 respective vertical stress of 50, 100, 200, 400, 800 and 1600 kPa; loading phase  
359 has been extended for about 30 minutes for low loads (that is 50, 100 and 200 kPa,  
360 as settlements were stabilized), and for 18 h for higher loads (that is 400, 800 and  
361 1600 kPa); the unloading phase has been stepped by reducing the total applied  
362 load to 800 kPa, then 200 kPa and finally to zero, carrying out settlement  
363 measurements for 24 hours at each step.

364 Figure 7 shows some examples of total settlement for the four different adopted curing  
365 timelines. The results can be interpreted following the main direction of one dimensional  
366 consolidation approach for soils, even a fundamental difference has to be outlined: grout  
367 presents a structure which is still chemically reactive and water contained in pores can be  
368 pushed aside (classical effect for soil grains) but can also migrate during reaction and  
369 therefore the expected properties at rest cannot be fulfilled. The classical approach by  
370 Casagrande (1936) can therefore be applied, even if with care.



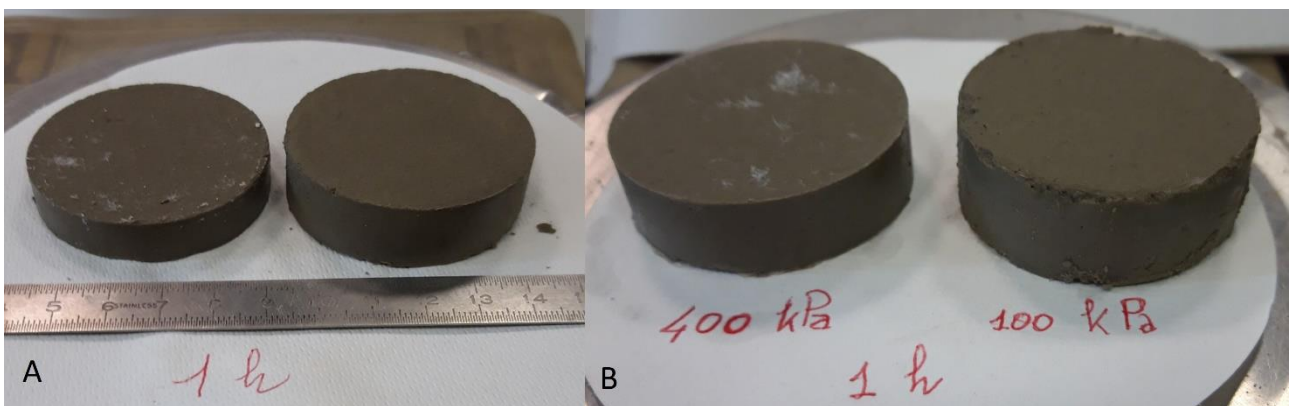
371  
 372 **Fig. 7. Example of raw data in log t vs settlement at different grout curing timelines,**  
 373 **obtained from oedometer testing (diameter 50 mm and height 20 mm). A) curing**  
 374 **time 1 hour under 100kPa load, B) curing time 24 hours under 800kPa load, C)**  
 375 **curing time 7 days under 1200kPa load, D) curing time 28 days under all loads.**

376 Figure 8 presents the comparison among the specimens respectively of net strain, due to  
 377 both mechanical and drainage process of deformation (consolidation), and the total  
 378 settlement (viscous effects) for two selected curing ages, 1 and 24 hours. These results  
 379 are interesting because they put in evidence that there is a relevant plastic deformation at  
 380 the various stress levels, and that is not recoverable, for the various loading levels; the  
 381 amount of recovered settlement after the unloading phase is low, sometimes negligible.  
 382 Besides, specimens before and after oedometer test exhibit a clear geometrical change  
 383 (see Fig. 9).



384

385 **Fig. 8. Comparison among the specimens respectively of net strain and total**  
 386 **settlement at 1 h and 24 h of curing. Net strain values refer to “consolidation” phase**  
 387 **of loading-unloading, while total settlement refers to the raw values at the beginning**  
 388 **and at the end of each cycle. A and B refers to 1 hour curing time, C and D to 24**  
 389 **hours curing time.**

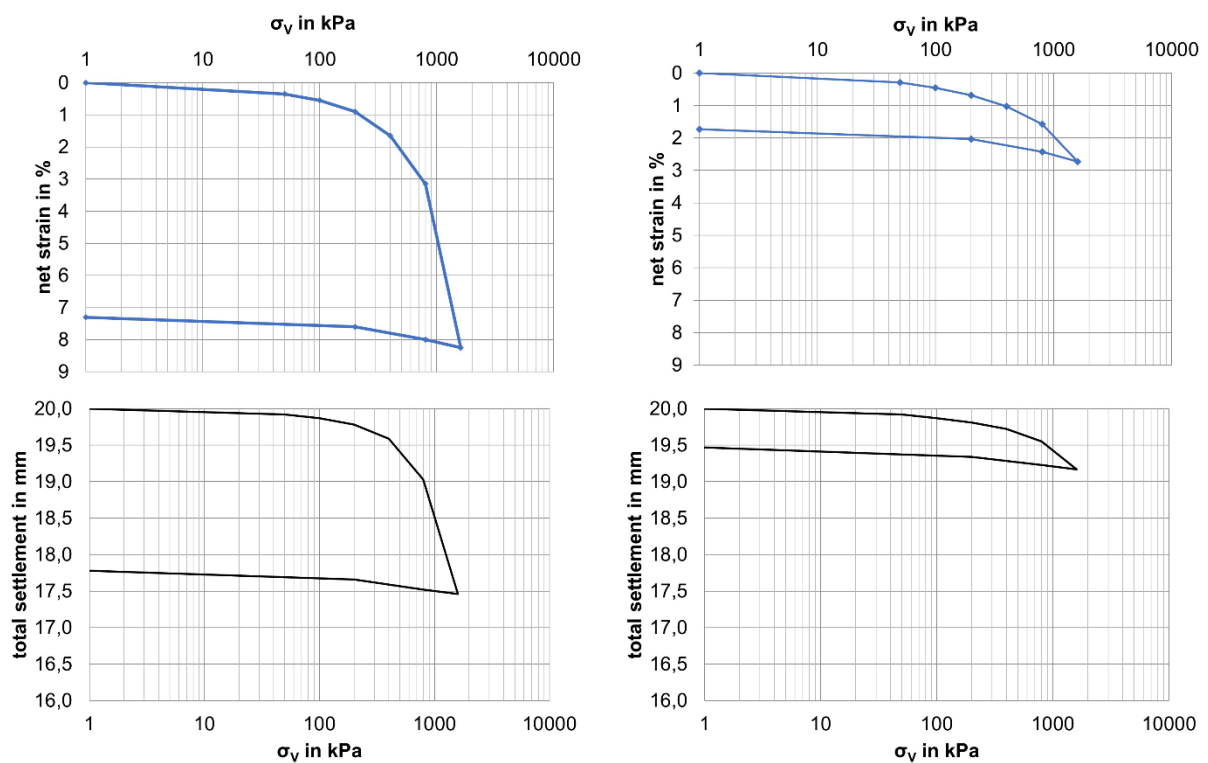


390

391 **Fig.9. A) Specimen before (at the right) and after (at the left) a loading –unloading**  
 392 **cycle at high stress levels. B) Comparison of specimens after cycle of loading-**

393 **unloading at 100 kPa and 400 kPa: the difference in the residual thickness due to**  
394 **plastic settlements is remarkable.**

395 Figure 10 summarize a typical stress-strain behaviour for the soil-like materials at the end  
396 of the curing period (28 days). A critical range of stress for the stability of the grout  
397 structure seems to confirm that grout has a meta-stable structure, due to diffusion of  
398 bentonite inside the material and to the initial high water/cement ratio.



399

400 **Fig. 10. The diagrams are showing for the two specimens tested after 28 days of**  
401 **curing (OED1, left and OED 2, right) for loading and unloading cycle. Net strain**  
402 **values refer to “consolidation” phase of loading-unloading, while total settlement**  
403 **refers to the raw values at the beginning and at the end of each cycle.**

404 Some interesting features arise from the diagrams showing the values of the constrained  
405 moduli, obtained in confined conditions (Fig. 11). It is shown that the curing time is  
406 affecting properties of the grout and its workability as well. Strength and stiffness are both

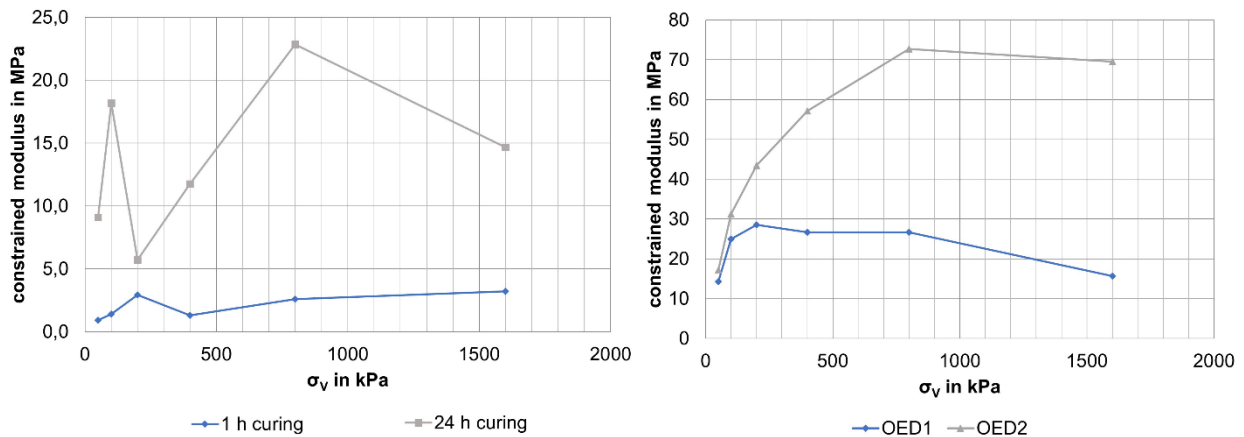
407 “mixing-sensitive”, and this fact should be taken into account for engineering application; in  
408 fact, on one side, changes in mixing energy, temperature, moisture and time for mixing  
409 can modify the structure, the behaviour and the properties of the grout. On the other side,  
410 at the scale of the machine, it is necessary that a suitable compromise is reached for the  
411 mixing timing: in fact water glass addition should be operated just to allow the quick setting  
412 of the gel and of the cementitious structure, but not so anticipated for the risk of clogging of  
413 the grout pipes and nozzles. The final result of a viscous grout to properly fill and support  
414 the gap between the lining extrados and the ground excavated profile is the goal.

415 Curing is affecting the values of constrained modulus, as it happened already for the  
416 uniaxial compressive test. Moreover, it is interesting that for short curing timelines, a peak  
417 value of the modulus appears (namely at 1h and 24 h). This fact seems to be in agreement  
418 with the external aspect of the grout, which is similar to a medium consistent clay at the  
419 beginning of the curing period, and that reaches the characteristics of a hard soil for long  
420 curing time. The presence of these peaks in the modulus graph was well described by  
421 Janbu (1969) in the case of fine-grained soils. Its importance is related to the local range  
422 of applied stress that is linked to pre-consolidation pressure. It is clear that such  
423 phenomenon cannot occur during the preparation of the grout, but this evidence can be  
424 interpreted as a “meta-stable pressure” for the grout structure “in formation”. This proposal  
425 is quite interesting as it can justify the clear change of behaviour for clay-like conditions of  
426 the grout. **The similarity to real soil behaviour is arising from the possibility to observe a  
427 good adherence to settlement vs time and vertical pressure vs strain of the loading steps  
428 of tested grout mix. Moreover the results in Fig.11 concerning the modulus vs the stress  
429 level are typical of consolidated clays. That is a convenient reason to make confident to  
430 approach with one-dimensional consolidation theory. For sure grout is an artificial material,  
431 with cemented bonds that are different from cohesion arising from water suction and**

432 surface membrane effect due to polarity of clay particles: the discussion on such difference  
 433 should be considered for specific laboratory comparison.

434

435



436

437 **Fig. 11. Scaled graphs showing the distribution of constrained moduli at different**  
 438 **curing ages (1 hour and 24 hours at left, 28 days at right) and depending on the**  
 439 **vertical applied stress. Note that the y-axis is different to better show the shape of**  
 440 **the graphs.**

441 As referred to the original thickness of the specimen (20 mm) and to the specific step in  
 442 the vertical effective stress ( $\Delta\sigma_v$ ), in the previous graphs the values of the constrained  
 443 moduli can be considered as tangent values. As far as the constrained modulus is  
 444 concerned (referring to the full value of applied vertical stress  $\sigma_v$ ), after 28 days of curing  
 445 time the following values have been measured (Tab. 2):

Secant constr. modulus at 28 d in MPa	$\sigma_v$ 50 kPa	$\sigma_v$ 100 kPa	$\sigma_v$ 200 kPa	$\sigma_v$ 400 kPa	$\sigma_v$ 800 kPa	$\sigma_v$ 1600 kPa
OED 1	14.3	18.2	22.2	24.2	25.4	19.4

OED 2	17.2	22.2	29.4	38.4	50.6	58.6
-------	------	------	------	------	------	------

446 **Table 2. The secant values of the constrained moduli at 28 days of curing are listed.**

447 Another relevant issue is concerning the lateral expansion of the grout under loading.  
448 Some data arise from the compression testing, showing that the Poisson coefficient “ $\nu$ ”  
449 exhibits generally low values. In order to find a confirmation of this behaviour, a correlation  
450 between oedometer results and compression results has been arranged, taking into  
451 account the basic correlation valid for linear elasticity and for homogenous and isotropic  
452 materials in constrained conditions:

$$453 \quad M_{constr} = \frac{(1-\nu)}{(1+\nu)(1-2\nu)} \cdot E \quad (3)$$

454 Where  $M_{constr}$  is the oedometer modulus,  $\nu$  is the Poisson ratio and  $E$  is the elastic  
455 modulus.

456 The cross checking of the raw data in the uniaxial compression tests and in the oedometer  
457 tests allows to obtain values of Poisson coefficient in the range of 0.03÷0.15, confirming  
458 the results obtained by direct measures during uniaxial compression tests. The selection of  
459 a proper value should follow some criteria such as:

- 460 • linearity of the stress – strain envelope;
- 461 • type of expected conditions of confinement in the real case;
- 462 • level of stress expected in site.

463 Nevertheless, this appear as one of the most sensitive features of the grout behaviour,  
464 thus requesting a larger data base of raw experimental data.

465 Some additional information can be obtained by means of a further processing of the  
466 available data. In order to measure the permeability, it was decided to indirectly obtain  
467 through an oedometer test, as for very low permeability values ( $10^{-8}$  m/s) it is preferable to  
468 use indirect tests (e.g. Colombo and Colleselli, 1996). The indirect coefficient of  
469 permeability  $k$  can be obtained by as combination of the consolidation coefficient  $C_V$  and  
470 of the coefficient of volume change  $m_v$  by adopting the formula  $k = C_V * m_v * \gamma_w$ . The  
471 intermediate terms can be obtained if some assumptions are taken into account: a) the  
472 behaviour of the grout during confined loading is similar to that of fine natural granular  
473 materials; b) the interpretation of raw data should follow the one-dimensional consolidation  
474 theory; c) the Casagrande method to interpret the rheology of the grout is valid to identify  
475 the compressibility features and characteristics of the grout; d) the general limitations on  
476 the validity of the indirect coefficient of permeability, known for soils, are maintained also  
477 for the artificial grout while carrying out the interpretation of the results. Following these  
478 statements, the values of  $k$  are presented in the Tab. 3.

Vertical stress in kPa	1 h curing time	24 h curing time	7 d curing time	28 d curing time	28 d curing time
				OED1	OED2
50	$1.35 \cdot 10^{-7}$	$2.15 \cdot 10^{-7}$	-	$2.75 \cdot 10^{-7}$	$2.85 \cdot 10^{-7}$
100	$4.32 \cdot 10^{-8}$	$7.16 \cdot 10^{-8}$	-	$1.56 \cdot 10^{-7}$	$1.78 \cdot 10^{-7}$
200	$8.87 \cdot 10^{-7}$	$9.41 \cdot 10^{-7}$	-	$2.26 \cdot 10^{-7}$	$1.11 \cdot 10^{-7}$
400	$2.25 \cdot 10^{-8}$	$3.21 \cdot 10^{-7}$	$1.25 \cdot 10^{-7}$ $2.73 \cdot 10^{-9}$	$2.39 \cdot 10^{-7}$	$8.42 \cdot 10^{-8}$
800	$3.35 \cdot 10^{-8}$	$1.63 \cdot 10^{-7}$	-	$2.30 \cdot 10^{-7}$	$6.53 \cdot 10^{-8}$
1200	-	-	$1.29 \cdot 10^{-7}$	-	-
1600	$1.09 \cdot 10^{-8}$	$9.07 \cdot 10^{-8}$		$2.61 \cdot 10^{-7}$	$6.63 \cdot 10^{-8}$

479 **Table 3. Values of indirect theoretical permeability coefficient  $k$  in cm/s.**

480 It is important to underline again the fact that the above listed values are obtained through  
481 an indirect procedure and not by means of a drainage test. The consequence of this fact is  
482 that an interpretation and an engineering judgement is necessary to properly adopt reliable  
483 values in practical design. The following issues should be taken into account: a) the order  
484 of magnitude of  $1.1 \cdot 10^{-7}$  cm/s to  $9.4 \cdot 10^{-7}$  cm/s seems reasonable for the majority of tested  
485 cases; b) the values at  $1.0 \cdot 10^{-8}$  to  $9.0 \cdot 10^{-8}$  cm/s are quite optimistic outside the laboratory  
486 scale; moreover, settlements and time-dependent movements for both ground and  
487 segmental lining can affect the global permeability; c) values in the order of  $10^{-9}$  cm/s  
488 seems to be unrealistic. As final consideration, it can be observed that the tested grout has  
489 low to very low permeability parameters for a wide range of operational stresses.

#### 490 *Auxiliary testing*

491 Together with data provided in the sheet for cylindrical specimens, some additional  
492 information arises from the specimens prepared for oedometer testing. In these cases,  
493 apparent unit weight is varying in the range 1.20 to 1.40 g/cm<sup>3</sup> for fresh and cured  
494 specimen respectively. Interesting is the reduction of apparent unit weight after loading-  
495 unloading cycle for fresh specimen at high level of consolidation pressure: the reduction  
496 moves to 0.75 to 1.08 g/cm<sup>3</sup>. After drying at natural environmental conditions, apparent  
497 unit weight for both cylindrical and disc specimen reduces to less than 0.80 g/cm<sup>3</sup>,  
498 reaching also 0.71 g/cm<sup>3</sup>; desiccated grout is friable and crispy. Soil pocket penetrometer  
499 (Soil Test model) has provided, for the first disc specimen, a penetration strength at 1 hour  
500 of 90 - 80 - 85 - 80 - 80 - 80 kPa; after 2 hours, the strength was increased to about 120 -  
501 120 - 125 kPa. The second disc specimen presented a penetration strength after 1 hour of  
502 about 70 - 60 - 85 kPa, and after 2 hours of about 125 - 150 - 90 - 140 - 90 - 110 kPa. Both  
503 specimens after 24 hours reached the full range of the soil pocket penetrometer at more

504 than 400 kPa; this same result was obtained on the lateral surface of the large diameter  
505 cylindrical specimen (75 mm).

### 506 **3. Simplified methods of tunnel segmental lining analysis**

507 Two methods for the behavior analysis of retaining structures are commonly used in the  
508 tunnel field: the convergence-confinement method and the Einstein and Schwartz method  
509 (1979). These methods have the advantage of being able to effectively evaluate the  
510 complex mechanism of interaction between the support and the walls of the tunnel, using a  
511 simplified approach that does not require the use of numerical calculation methods.

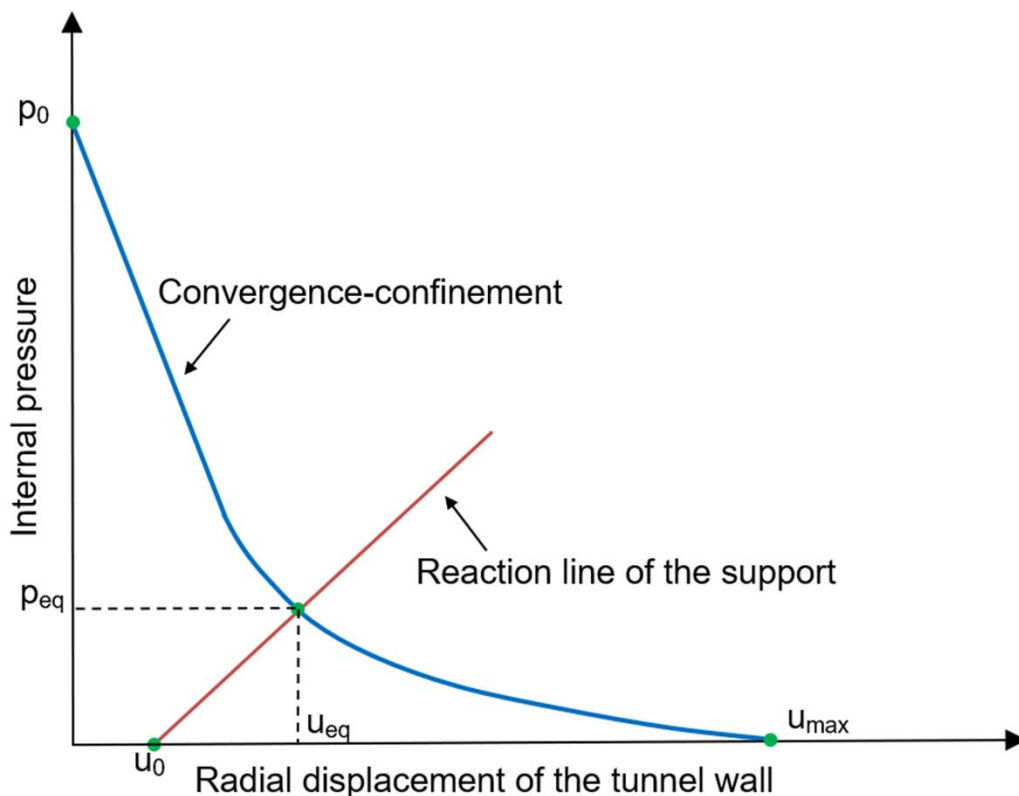
512 More specifically, the convergence-confinement method is able to evaluate the final entity  
513 of the loads acting on the support structure,  $p_{eq}$  through the intersection of the  
514 convergence-confinement curve and the reaction line representing the support structure,  
515 determining the displacement of the tunnel wall in the radial direction ( $u_{eq}$ ) (Fig. 12). The  
516 convergence-confinement method is based on the following fundamental assumptions:

- 517 • Circular geometry of the tunnel and radial symmetry of the problem analyzed in the  
518 two dimensions (vertical section)
- 519 • Deep tunnel hypothesis (depth of the tunnel relatively high compared to its radius)
- 520 • Homogeneous mechanical characteristics of the rock around the tunnel;
- 521 • Hydrostatic initial stress state (undisturbed)  $p_0$  with lateral earth coefficient at rest  
522  $K_0 = 1$ .

523 The main problem in using the convergence-confinement method lies in being able to  
524 correctly simulate the three-dimensional nature of the support loading mechanism in a two-  
525 dimensional model. The fundamental parameter for this purpose is the displacement  $u_0$  of  
526 the tunnel wall when the support structure is installed. Various calculation techniques are

527 available in the literature capable of producing an estimate of this parameter and therefore  
528 having reliable results from the convergence-confinement method.

529 Fig. 12 shows the results of the convergence-confinement method through the analysis of  
530 two curves: the convergence-confinement curve and the reaction line of the supporting  
531 structure.  $p$  is the pressure inside the tunnel, acting on the walls,  $u_R$  is the radial  
532 displacement of the tunnel wall,  $p_0$  is the lithostatic stress present in the rock,  $u_0$  is the  
533 radial displacement of the tunnel wall upon installation of the support;  $p_{eq}$  and  $u_{eq}$  are  
534 respectively the final load acting on the support structure and the final displacement of the  
535 tunnel wall in the presence of the support structure and  $u_{max}$  is the maximum  
536 displacement of the tunnel wall in the absence of supports.



537

538 **Fig. 12 Results of the convergence-confinement method through the analysis of two**  
539 **curves: the convergence-confinement curve and the reaction line of the supporting**  
540 **system.**

541 In the simplest case of ideal elastic-plastic behavior of the rock and Mohr-Coulomb failure  
542 criterion, the convergence-confinement curve is expressed by the following relationship  
543 (Oreste, 2009):

544 For  $p < [p_0 \cdot (1 - \sin(\varphi)) - c \cdot \cos(\varphi)]$  :

545  $u_R =$

$$546 \frac{1+\nu}{E} \cdot \left\{ \left[ \frac{R_{pl}^{N_\Psi+1}}{R^{N_\Psi}} \cdot \sin(\varphi) + (1 - 2 \cdot \nu) \cdot \left( \frac{R_{pl}^{N_\Psi+1}}{R^{N_\Psi}} - R \right) \right] \cdot \left( p_0 + \frac{c}{\tan(\varphi)} \right) - \frac{1+N_\Phi \cdot N_\Psi - \nu \cdot (N_\Psi+1) \cdot (N_\Phi+1)}{(N_\Phi+N_\Psi) \cdot R^{(N_\Phi-1)}} \cdot \right.$$

$$547 \left. \left( \frac{R_{pl}^{(N_\Phi+N_\Psi)}}{R^{N_\Psi}} - R^{N_\Phi} \right) \cdot \left( p + \frac{c}{\tan(\varphi)} \right) \right\} \quad (4)$$

548 where  $R_{pl}$  is the plastic radius of the tunnel:

$$549 R_{pl} = R \cdot \left[ \frac{\left( p_0 + \frac{c}{\tan(\varphi)} \right) \cdot (1 - \sin(\varphi))}{p + \frac{c}{\tan(\varphi)}} \right]^{\frac{1}{(N_\Phi-1)}} \quad (5)$$

$$550 N_\Phi = \frac{1 + \sin(\varphi)}{1 - \sin(\varphi)} \quad (6)$$

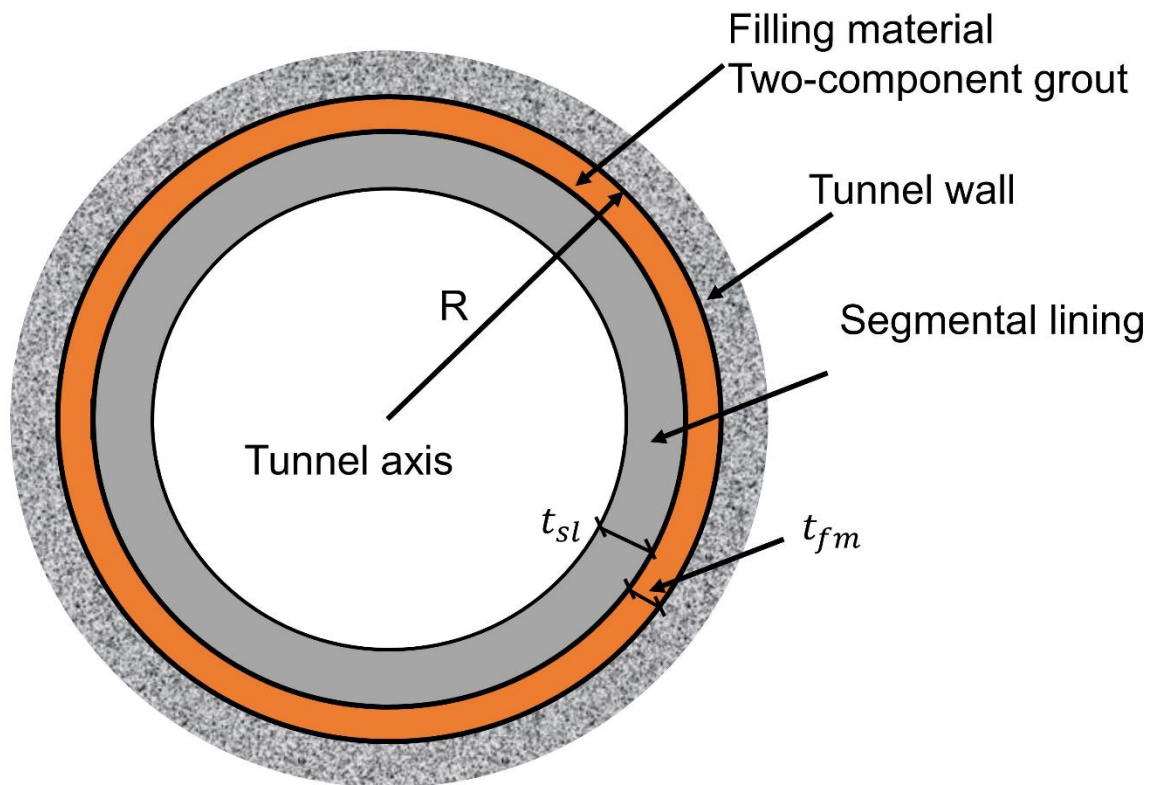
$$551 N_\Psi = \frac{1 + \sin(\Psi)}{1 - \sin(\Psi)} \quad (7)$$

552  $R$  is the tunnel radius,  $c$ ,  $\varphi$  and  $\Psi$  are respectively the cohesion, friction angle and  
553 dilatancy of the rock mass,  $E$  and  $\nu$  are respectively the elastic modulus and the Poisson  
554 ratio of the rock mass.

555 For  $p > [p_0 \cdot (1 - \sin(\varphi)) - c \cdot \cos(\varphi)]$ :

556 
$$u_R = \frac{1+\nu}{E} \cdot (p_0 - p) \cdot R \quad (8)$$

557 The reaction line of the support in the case of a segmental lining must take into account  
 558 the presence of the filling material in the gap between the segmental lining and the tunnel  
 559 wall (Fig. 13).



560

561 **Fig. 13. Geometric sketch of the support system consisting of segmental lining and**  
 562 **filling material within a circular tunnel. Legend:  $R$ : radius of the tunnel;  $t_{sl}$ :**  
 563 **thickness of the segmental lining;  $t_{fm}$ : thickness of the filling material (not to scale).**

564 Similarly to what was developed for the shotcrete lining plus inner steel set support system  
 565 (Oreste, 2003; Oreste et al., 2018a, 2018b), it is possible now to define for the reaction line  
 566 of the support the stiffness,  $k_{sys}$ , of the system consisting of the segmental lining and the  
 567 annulus of the filling material with the following relationship:

$$k_{sys} = \frac{2 \cdot E_{fm} \cdot (1 - \nu_{fm}) \cdot R \cdot \left[ \frac{E_{fm}}{(1 + \nu_{fm})} + (R - t_{fm}) \cdot k_{sl} \right]}{E_{fm} \cdot (1 - 2 \cdot \nu_{fm}) \cdot R^2 + (R - t_{fm})^2 \cdot \left[ E_{fm} + (1 - 2 \cdot \nu_{fm}) \cdot (1 + \nu_{fm}) \cdot k_{sl} \cdot t_{fm} \cdot \left( 1 + \frac{R}{(R - t_{fm})} \right) \right]} - \frac{E_{fm}}{(1 + \nu_{fm}) \cdot R} \quad (9)$$

where:

$$k_{sl} = \frac{E_{sl}}{(1 + \nu_{sl})} \cdot \frac{(R - t_{fm})^2 - (R - t_{fm} - t_{sl})^2}{(1 - 2 \cdot \nu_{sl}) \cdot (R - t_{fm})^2 + (R - t_{fm} - t_{sl})^2} \cdot \frac{1}{(R - t_{fm})} \quad (10)$$

$E_{fm}$  and  $\nu_{fm}$  are respectively the elastic modulus and the Poisson's ratio of the filling material;  $E_{sl}$  and  $\nu_{sl}$  are respectively the elastic modulus and the Poisson's ratio of the segmental lining;  $t_{fm}$  and  $t_{sl}$  are respectively the thickness of the filling material and segmental lining;  $k_{sl}$  is the stiffness of the segmental lining. As can be seen from the previous equations, knowing the characteristics of the filling material (thickness, elastic modulus and Poisson's ratio) it is possible to identify the stiffness of the support system which allows to draw the reaction line of the support. In fact, the stiffness of the system represents the inclination of the reaction line with respect to the horizontal axis in the diagram of Fig. 12.

Since the elastic modulus of the filling material  $E_{fm}$  varies significantly during the setting period and, therefore, during the loading of the segmental lining, it is necessary to define a representative average value for the considered period. To evaluate it, it is necessary to know not only the trend of the elastic modulus of the filling material over time during the setting period (curing time), but also the advancement speed of the TBM inside the tunnel and the duration of the various excavation and installation of supports. It is a question of addressing this problem with the same approach used for the evaluation of the average elastic modulus of shotcrete during the loading phase of the lining in the tunnel, with the advancement of the excavation phase (e.g. Oreste et al., 2019).

588 Another very widespread calculation method in the analysis of the behavior of the  
589 supporting structures of tunnels is the method of Einstein and Schwartz (1979). This  
590 method assumes an annular support continuously connected with the wall of a deep and  
591 circular tunnel. Two different cases were examined by the authors: the full slip case and  
592 the no-slip case. The solution obtained allows to consider the interaction between the  
593 supporting structure and the rock mass around the tunnel, assuming a material with an  
594 elastic behavior both for the rock and for the support. For the analysis of the segmental  
595 lining with the filling material present in contact with the rock wall, it is more appropriate to  
596 refer to the full-slip case, which provides the following equations for the evaluation of the  
597 maximum bending moment,  $M_{max}$ , and the normal force,  $N$ , present in the lining (in  
598 particular in the center of the crown and in the middle of the side-wall) (Einstein and  
599 Schwartz, 1979; Guan et al., 2015):

$$600 \quad M_{max} = (1 + \xi) \cdot \frac{p_{eq} \cdot R^2 \cdot (1 - K_0)}{(1 + K_0) \cdot (1 - a_0^*) + (1 - K_0) \cdot (3 - 6 \cdot a_2^*)} \cdot (1 - 2 \cdot a_2^*) \quad (11)$$

$$601 \quad N_{crown} = \frac{p_{eq} \cdot R \cdot (1 + K_0)}{(1 + K_0) \cdot (1 - a_0^*) + (1 - K_0) \cdot (3 - 6 \cdot a_2^*)} \cdot (2 \cdot a_2^* - a_0^*) \quad (12)$$

$$602 \quad N_{sidewall} = \frac{p_{eq} \cdot R \cdot (1 + K_0)}{(1 + K_0) \cdot (1 - a_0^*) + (1 - K_0) \cdot (3 - 6 \cdot a_2^*)} \cdot (2 - a_0^* - 2 \cdot a_2^*) \quad (13)$$

603 where:

$$604 \quad a_0^* = \frac{C^* \cdot F^* \cdot (1 - \nu)}{C^* + F^* + C^* \cdot F^* \cdot (1 - \nu)} \quad (14)$$

$$605 \quad a_2^* = \frac{(F^* + 6) \cdot (1 - \nu)}{2 \cdot F^* \cdot (1 - \nu) + 6 \cdot (5 - 6 \cdot \nu)} \quad (15)$$

$$606 \quad C^* = \frac{E \cdot R \cdot (1 - \nu_s^2)}{E_s \cdot A_s \cdot (1 - \nu^2)} \quad (16)$$

607 
$$F^* = \eta \cdot \frac{E \cdot R^3 \cdot (1 - \nu_s^2)}{E_s \cdot I_s \cdot (1 - \nu^2)} \quad (17)$$

608  $p_{eq}$  is vertical load acting on the support structure in the vertical direction, in  
609 correspondence with the crown tunnel (evaluated, for example, through the convergence-  
610 confinement method);

611  $K_0$  is the lateral earth pressure at rest in the rock, in the initial undisturbed conditions;

612  $R$  is the tunnel radius;

613  $E$  and  $\nu$  are respectively the elastic modulus and the Poisson ratio of the rock;

614  $E_s$  and  $\nu_s$  are respectively the elastic modulus and the Poisson ratio of the support  
615 structure;

616  $A_s$  and  $I_s$  are respectively the area and moment of inertia of the cross section of the  
617 support, through a plane passing through the axis of the tunnel. The cross section  
618 therefore has a rectangular section, whose width is equal to 1 m in the direction of the  
619 tunnel axis and the height is equal to the thickness of the support

620  $C^*$  and  $F^*$  are compressibility ratio and flexibility ratio of the support, respectively.

621  $\xi$  is the incremental coefficient that takes into account the transfer of stresses from one  
622 ring to the adjacent one, in correspondence with the longitudinal joints of the segmental  
623 lining. Guan et al. (2015) were able to note how this parameter varies from 0.44 to 0.46,  
624 with an intermediate value equal to 0.45 and is not influenced by the characteristics of the  
625 ground and the depth of the tunnel, but only by the geometric and mechanical  
626 characteristics of the longitudinal and transverse joints of the segmental lining;

627  $\eta$  is reduction coefficient taking into account the presence of longitudinal joints in  
628 segmental lining. In this regard Guan et al. (2015) suggest reducing the bending stiffness  
629 by a coefficient  $\eta$ , which was found to vary between 0.4 and 0.7, with an intermediate  
630 value of 0.55. This coefficient was found to be higher in more compact soils and for  
631 tunnels at greater depths.

632 The maximum moment  $M_{max}$  assumes the same value in the center of the crown and on  
633 the sidewall, but a different sign: the one in the crown will be considered positive and the  
634 one on the sidewall negative, for the typical case in which  $K_0$  is less than 1; if  $K_0$  is greater  
635 than 1, the moment on the sidewall will be positive and the moment at the crown tunnel is  
636 negative.

637 The normal forces are different in the tunnel crown and on the sidewall: by associating the  
638 values of the normal forces with the bending moments, it is possible to check the  
639 hypothesized lining in the two critical points highlighted above: the center of the crown  
640 tunnel and the center of the. In the verification process, the thickness of the segmental  
641 lining is changed to obtain a value considered compatible with the safety and stability  
642 conditions of the support structure and the tunnel.

643 When the use of segmental lining as a support structure is planned, it is important to  
644 consider composite support is obtained which also includes a ring of filling material  
645 between the segmental lining and the wall of the tunnel. The evaluation of the equivalent  
646 elastic modulus of the support must consider the presence of the two materials (Fig. 13).  
647 Assuming the preservation of the flat sections of the lining (segmental lining and filling  
648 material), it is possible to identify the equivalent elastic modulus  $E_{s,eq}$  of the support. This  
649 equivalent elastic modulus turns out to be different in relation to the bending and

650 compression of the lining and, therefore, must be evaluated through different equations  
651 with reference to the compressible ratio  $C^*$  and the flexibility ratio  $F^*$ .

652 Equivalent elastic modulus of the support with reference to the compressibility ratio  $C^*$ :

$$653 \quad E_{s,eq(C^*)} = E_{sl} + E_{fm} \cdot \frac{t_{fm}}{t_{sl}} \quad (18)$$

654 Equivalent elastic modulus of the support with reference to the flexibility ratio  $F^*$ :

$$655 \quad E_{s,eq(F^*)} = \frac{4}{t_{sl}^3} \cdot \left\{ E_{sl} \cdot [y_0^3 + (t_{sl} - y_0)^3] + E_{fm} \cdot \left[ (t_{sl} + t_{fm} - y_0)^3 - (t_{sl} - y_0)^3 \right] \right\} \quad (19)$$

656 Where:

$$657 \quad y_0 = \frac{E_{sl} \cdot t_{sl}^2 + E_{fm} \cdot (t_{fm}^2 + 2 \cdot t_{sl} \cdot t_{fm})}{2 \cdot (E_{sl} \cdot t_{sl} + E_{fm} \cdot t_{fm})} \quad (20)$$

658 Being  $y_0$  the distance of the neutral axis of the section from the intrados of the segmental  
659 lining.

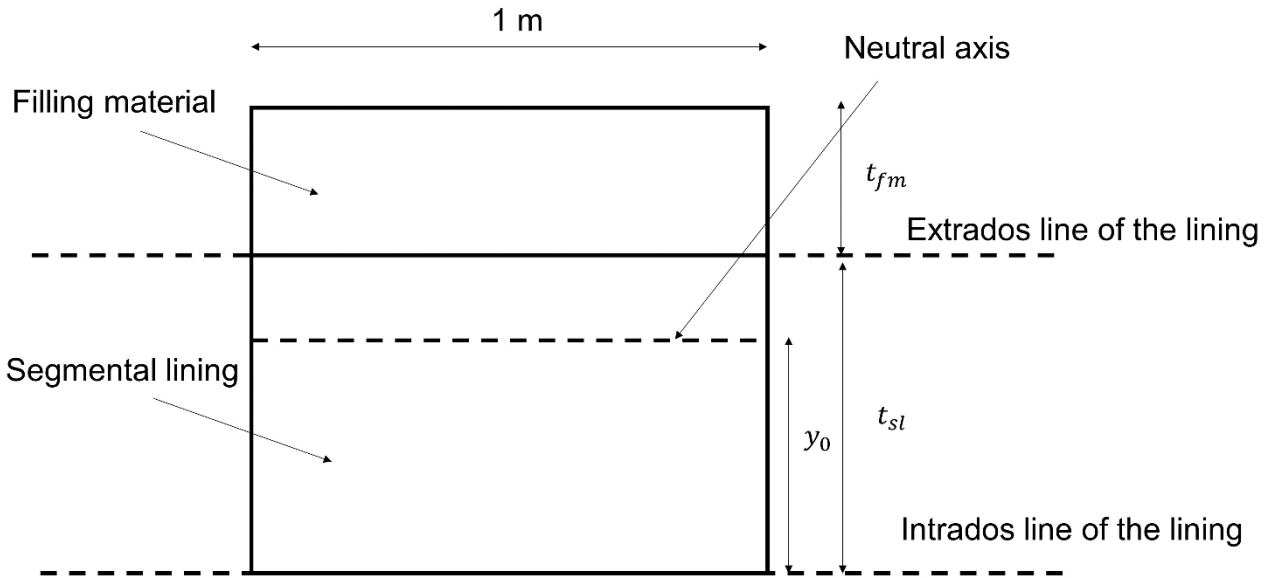
660 The values of the equivalent elastic modules reported above were obtained assuming an  
661 equivalent support of thickness equal to the thickness of the segmental lining:  $t_{s,eq} = t_{sl}$ .

662 For this reason, the values of the area of the support section  $A_s$  and of the moment of  
663 inertia  $I_s$  must be evaluated with the following two equations:

$$664 \quad A_s = b_s \cdot t_{sl} \quad (21)$$

$$665 \quad I_s = \frac{b_s \cdot t_{sl}^3}{12} \quad (22)$$

666 Where  $b_s$  is the width of the support section in the direction of the tunnel axis, considered  
667 equal to 1 m.



668

669 **Fig. 14. Cross section of the segmental lining with the presence of the filling**  
 670 **material. Legend:  $t_{sl}$  is thickness of the segmental lining;  $t_{fm}$  is thickness of the**  
 671 **filling material;  $y_0$  is distance of the neutral axis of the section from the intrados of**  
 672 **the segmental lining.**

673 Based on the calculations that can be developed considering the equivalent support  
 674 described above, it will be possible to identify the maximum moments along the  
 675 development of the support and the normal forces at the center of the crown and the  
 676 sidewall. Starting from these results, it will be possible to determine the circumferential  
 677 stresses  $\sigma_{\vartheta}$  in the segmental lining and in the filling material using the following equations.

678 Circumferential stress at the extrados of the segmental lining  $\sigma_{\vartheta,sl,ex}$  due to moment  $M$ :

$$679 \quad \sigma_{\vartheta,sl,ex} = \frac{12 \cdot M}{E_{s,eq(F^*)} \cdot b_s \cdot t_{sl}^3} \cdot (t_{sl} - y_0) \cdot E_{sl} \quad (23)$$

680 Circumferential stress at the intrados of the segmental lining  $\sigma_{\vartheta,sl,in}$  due to moment  $M$ :

$$681 \quad \sigma_{\vartheta,sl,in} = -\frac{12 \cdot M}{E_{s,eq(F^*)} \cdot b_s \cdot t_{sl}^3} \cdot y_0 \cdot E_{sl} \quad (24)$$

682 Maximum circumferential stress on the extrados of the filling material  $\sigma_{\vartheta, fm, ex}$  due to the  
683 moment  $M$ :

$$684 \quad \sigma_{\vartheta, fm, ex} = \frac{12 \cdot M}{E_{s, eq(F^*)} \cdot b_s \cdot t_{sl}^3} \cdot (t_{fm} + t_{sl} - \gamma_0) \cdot E_{fm} \quad (25)$$

685 Constant stress in the segmental lining section due to the normal force  $N$ :

$$686 \quad \sigma_{\vartheta, sl} = \frac{E_{sl}}{E_{s, eq(C^*)}} \cdot N \quad (26)$$

687 Constant stress in the section of the filling material due to the normal force  $N$ :

$$688 \quad \sigma_{\vartheta, fm} = \frac{E_{fm}}{E_{s, eq(C^*)}} \cdot \frac{t_{fm}}{t_{sl}} \cdot N \quad (27)$$

689 The stress effects of the bending moment  $M$  and the normal force  $N$  must be summed  
690 algebraically to obtain the overall stress state in the filling material and in the segmental  
691 lining; in addition to the circumferential stresses, the radial stresses present in the two  
692 materials must be considered:  $p_{eq}$  at the extrados of the filling material and segmental  
693 lining and 0 at the intrados of the segmental lining. The overall stress state has to be  
694 compared to the strength of the material (the limit stress state), according to the Mohr-  
695 Coulomb strength criterium:

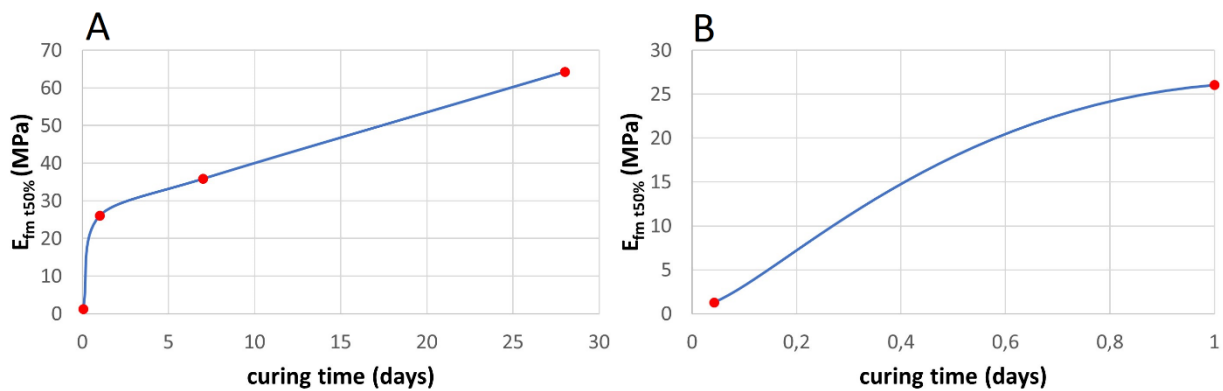
$$696 \quad \sigma_{lim} = UCS + \frac{1 + \sin(\varphi)}{1 - \sin(\varphi)} \cdot \sigma_r \quad (28)$$

697 Where  $UCS$  and  $\varphi$  are respectively the uniaxial compression strength and the friction angle  
698 of the material (concrete or filling material) and  $\sigma_r$  is the radial stress in the point where the  
699 stress state is evaluated during the design of the support structure (extrados of the filling  
700 material annulus, extrados or intrados of the segmental lining).

701 The knowledge of the overall stress state in the critical points of the support system allows  
702 to proceed to the verifications regarding the strength of the materials and, therefore, to the  
703 design of the segmental lining through the definition of its thickness and the internal  
704 reinforcement necessary to absorb the developing bending moments.

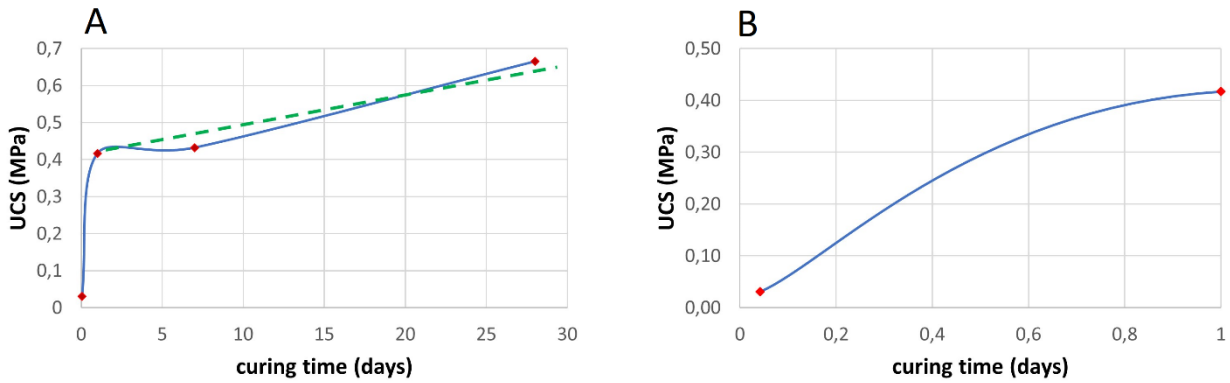
#### 705 4. The effect of the two-component grout on the behavior of the tunnel 706 segmental lining

707 From the laboratory tests on the two-component grout used as filling material, it is possible  
708 to detect how the value of the Poisson's ratio remains relatively low and uncertain (variable  
709 in the range 0.03-0.15) during the curing time. Besides, both the elastic modulus of the  
710 material and the UCS show a complex trend over time, described by the trends shown in  
711 Figs. 15 and 16. The values plotted in the figures are the average values between those  
712 measured in the laboratory tests of uniaxial compression for the different maturation times  
713 analyzed: 1 h (i.e. 0.04167 d), 1 day, 7 days, 28 days.



714

715 **Fig. 15. Trend of the tangent elastic modulus for a stress state equal to 50% of the**  
716 **uniaxial compressive strength ( $E_{fm,t 50\%}$ ) as the curing time varies. A): full time**  
717 **interval (0-28 days); B): detail on the first day of curing time (0-1 days).**



718

719 **Fig. 16. Trend of uniaxial compressive strength (UCS) as the curing time varies. A):**  
 720 **full time interval (0-28 days); B): detail on the first day of curing time (0-1 days).**  
 721 **Legend: dotted line: hypothetical linear trend for the period following the first day of**  
 722 **curing.**

723 More specifically, it is possible to hypothesize for the elastic modulus and for the UCS a  
 724 strong increase in the first day of curing and a linear trend for the subsequent period, up to  
 725 the 28 days of curing. On the first day of curing, it is plausible to hypothesize a parabolic  
 726 trend of the curves shown in the previous figures (Figs. 15 and 16). Assuming that the  
 727 parabolic curves connect with the straight lines for a curing time equal to 1 day and that  
 728 the additional condition that set UCS and  $E_{fm,t 50\%}$  zero for the time equal to  $t = 0$  is valid,  
 729 we obtain the following equations that allow us to describe the trends of the elastic  
 730 modulus and of the UCS over time, according to the parabola-trapezium scheme.

731  $E_{fm,t 50\%}$  in the period 0-1 day:

$$732 \quad E_{fm,t 50\%} = -5,7713 \cdot t^2 + 31,839 \cdot t \quad (29)$$

733  $E_{fm,t 50\%}$  in the period 1-28 days:

$$734 \quad E_{fm,t 50\%} = 1,4274 \cdot (t - 1) + 26,0667 \quad (30)$$

735 UCS in the period 0-1 day:

$$736 \quad UCS = -0,3329 \cdot t^2 + 0,74989 \cdot t \quad (31)$$

737 UCS in the period 1-28 days:

$$738 \quad UCS = 0,0089 \cdot (t - 1) + 0,417 \quad (32)$$

739 The identification of the average elastic modulus of the  $E_{fm}$  of the filling material during the  
740 loading of the segmental lining (with the advancement of the excavation face) is of great  
741 importance, as this parameter has a great influence on the stiffness of the  $k_{sys}$  system  
742 and, therefore, on the load induced on the segmental lining (Fig. 12). Another fundamental  
743 parameter is the thickness of the filling material  $t_{fm}$ . In order to investigate the influence of  
744 these parameters and the Poisson's ratio of the filling material  $\nu_{fm}$  a parametric analysis  
745 was developed, proceeding with the calculation of the stiffness of the  $k_{sys}$  system (eq. 9)  
746 considering all the following values of the influencing parameters, within the ranges of  
747 variability obtained from the laboratory tests described in this paper or from the scientific  
748 literature:

- 749 • Tunnel radius  $R$ : 2, 3.5 and 5 m;
- 750 • Elastic modulus of the filling material  $E_{fm}$ : 15, 30 and 45 MPa;
- 751 • Poisson's ratio of the filling material  $\nu_{fm}$ : 0.03, 0.09 and 0.15;
- 752 • Thickness of the filling material  $t_{fm}$ : 0.12, 0.18 and 0.24 m;
- 753 • Thickness of the segmental lining  $t_{sl}$ : 0.3 and 0.4 m.

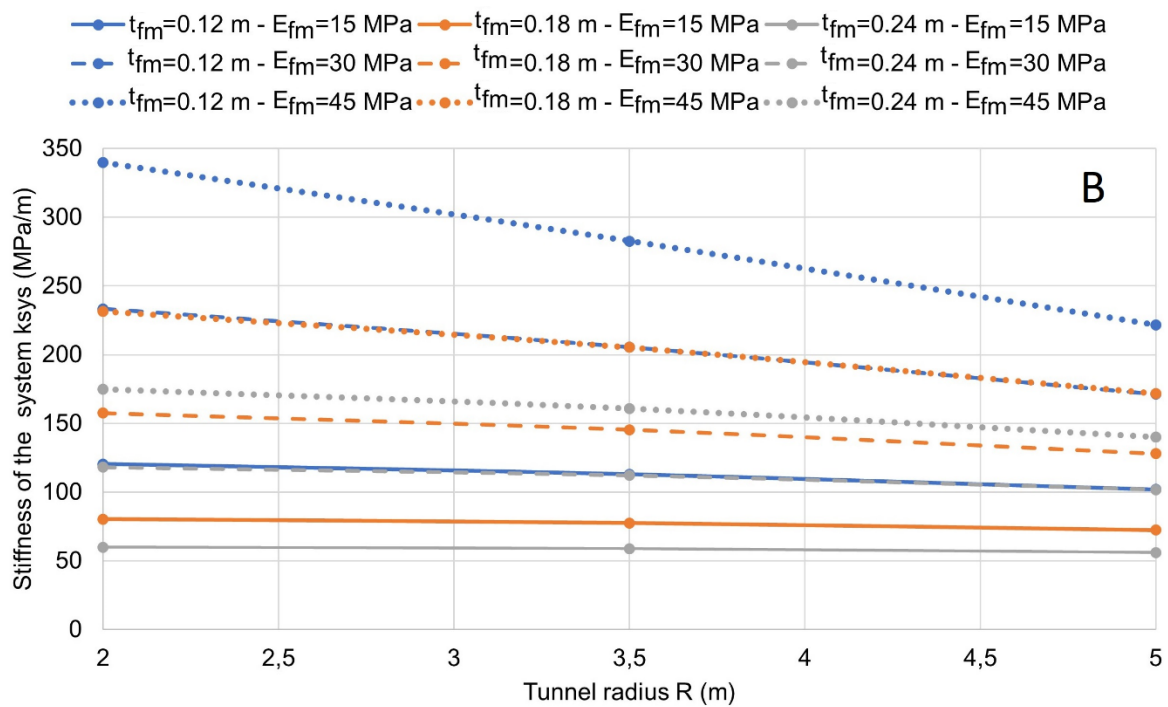
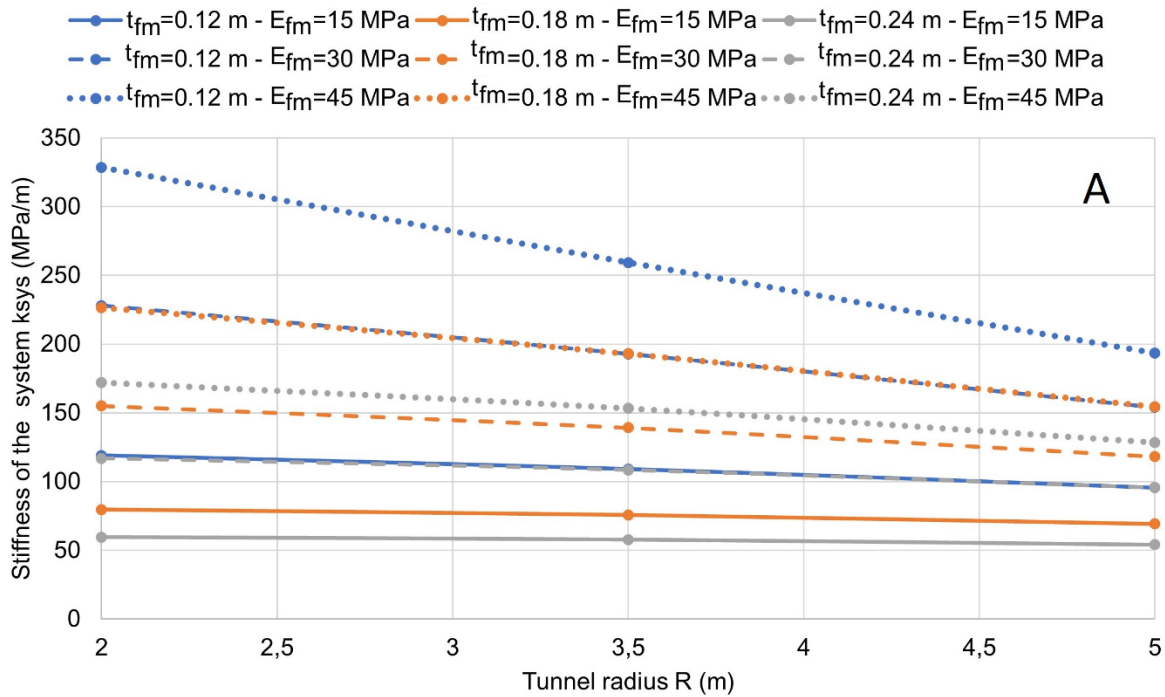
754 For the concrete forming the segmental lining, an elastic modulus  $E_{sl}$  of 30,000 MPa and a  
755 Poisson's ratio  $\nu_{sl}$  of 0.15 were considered. On the basis of the 162 analyzes carried out, it  
756 was possible to detect how the Poisson's ratio of the filling material has little influence on

757 the stiffness  $k_{sys}$  of the system in all the examined cases. For this reason, it is possible to  
758 plot the results obtained by neglecting this parameter, assuming it equal to 0.09, the  
759 intermediate value of the variability interval detected by laboratory tests (0.03-0.15).

760 Figure 17 (A and B) shows the values of the stiffness of the support system  $k_{sys}$  as the  
761 radius of the tunnel  $R$  varies, for the different values of  $E_{fm}$  and  $t_{fm}$  considered,  
762 respectively for a thickness of the segmental lining of 0.3 and 0.4 m.

763

764



765

766 **Fig. 17. Trend of the stiffness of the support system (segmental lining + filling**  
 767 **material annulus)  $k_{sys}$  as the tunnel radius  $R$  varies, for different values of the elastic**  
 768 **modulus  $E_{fm}$  and the thickness  $t_{fm}$  of the filling material, for the case of segmental**  
 769 **lining with a thickness of 0.3 m (A) and 0.4 m (B).**

770 From Fig. 17, it can also be seen that the radius of the tunnel  $R$  does not have a  
771 detectable influence on the stiffness of the system when the values of  $E_{fm}$  are low and  
772 those of  $t_{fm}$  high. Furthermore, for small tunnel radii, the thickness of the segmental lining  
773 does not affect the rigidity of the system. Once the correct value of the stiffness of the  $k_{sys}$   
774 system has been identified from the graphs of Fig. 17, it is possible through the  
775 convergence-confinement method to obtain an estimate of the load  $p_{eq}$  acting on the  
776 support system, in order to proceed with the design of the segmental lining and the  
777 definition of its thickness. In some cases, it is necessary to limit the load acting on the  
778 support system, to avoid an excessive stress state induced in the concrete constituting the  
779 segmental lining. This is the case of tunnels at great depths, for which it is possible to  
780 intervene appropriately on the thickness of the filling ring (increasing it) and on the  
781 mechanical characteristics of the filling material (limiting the elastic modulus) in order to  
782 obtain a low  $k_{sys}$  stiffness and, therefore, reduced load values on the support system.

783 In order to obtain a low elastic modulus value of the filling material, appropriate additives  
784 (e.g. higher retarder dosage) of the two-component material can be used or the excavation  
785 machine's advancement speed can be increased (if the technical conditions allow it), in  
786 order to load the segmental lining in relatively short times, when still the filling material  
787 shows limited mechanical parameters.

788 The design of the segmental lining proceeds with calculation methods that allow to study  
789 the development of the bending moments and of the axial forces along the development of  
790 the support, starting from the load  $p_{eq}$  that can be evaluated with the convergence-  
791 confinement method. Among the most common is the method of Einstein and Schwartz  
792 (1979), whose stiffness parameters  $C^*$  and  $F^*$  (the compressibility ratio and flexibility ratio  
793 of the support, respectively) were illustrated previously.

794 Also in this case, an extensive parametric analysis has been developed on the parameters  
795 that influence the coefficients  $C^*$  and  $F^*$  in order to verify the effect of the presence of the  
796 filling material on the behavior of the support structure.

797 The same values already used in the analysis relating to the stiffness  $k_{sys}$  of the system  
798 have now been adopted, with the addition of 3 different values of the elastic modulus of  
799 the rock mass: 3,162 MPa (relative to a rock mass having GSI = 30), 10,000 MPa (GSI =  
800 50) and 31,622 MPa (GSI = 70), where GSI is the Geological Strength Index of the rock  
801 mass (Hoek, 1994; Hoek et al., 1995; Hoek and Brown, 1997; Serafim and Pereira, 1983) .

802 The total of the performed analyzes was therefore equal to 486. It was possible to verify  
803 that in all cases the effect of the presence of the filling material ring is always less than 1.5  
804 ‰ on parameter  $C^*$  and always less than 1.5% on parameter  $F^*$ . In practical terms,  
805 therefore, in the analysis of the behavior of segmental lining through the Einstein and  
806 Schwartz method, it is possible to neglect the presence of the filling material ring in the  
807 evaluation of bending moments and normal forces acting on segmental lining. The design  
808 of the segmental lining can therefore proceed quickly, evaluating the stress state induced  
809 in the segmental lining, for different values of its thickness, after having calculated the  
810 acting bending moments and the normal forces.

## 811 **5. Conclusions**

812 Where a two-component grout is used during TBM excavation, the mechanical properties  
813 evolve over the time immediately after the injection, just during the loading of the linings. It  
814 is, therefore, important to be able to analyze the mechanical behavior of this filling  
815 material, in order to evaluate the effects of its presence on the stress state induced in  
816 segmental lining. An extensive laboratory program has been performed considering a  
817 particular mix-design of a two-component grout. Uniaxial compression tests and

818 oedometer tests, were carried out and allowed to characterize this type of material from a  
819 mechanical point of view over time. In particular, the stiffness (elastic modulus, Poisson's  
820 ratio, oedometer modulus) and the strength parameters (uniaxial compressive strength,  
821 friction angle and cohesion) were evaluated during the curing period of the material. The  
822 test campaign showed a certain sensitivity of the material to the preparation methods of  
823 the mixture and in particular in the gel formation phase with the mixing of the two  
824 components. The material presents a relatively modest density of the material obtained,  
825 due to a relatively high water/cement ratio, an elastic-plastic behavior of the material of the  
826 "softening" type, and specific compression threshold levels observed in the oedometer  
827 test, beyond which water seems to be expelled from the pores and a failure of the solid  
828 skeleton previously formed appears, with the consequent appearance of irreversible  
829 deformations.

830 Constrained compression has shown the role of a metastable structure in the formed  
831 grout, that determines a change of the settlement rate when a transition pressure is  
832 reached (meta stable pressure).

833 A detailed analysis of the influence of the filling material on the behavior of segmental  
834 lining was carried out using two widespread methods of calculating the tunnel support  
835 structures: the convergence-confinement method and the Einstein and Schwartz (1979)  
836 method. In particular, for the convergence-confinement method, the stiffness of the  
837 support system (segmental lining + filling ring) was evaluated. It has been noted how this  
838 stiffness of the support system can significantly affect the value of the load acting on the  
839 segmental lining. For the method of Einstein and Schwartz the stiffness coefficients of the  
840 lining were obtained, taking into account the presence of the filling material ring. An  
841 extensive parametric analysis allowed to identify the effects of the presence of the filling  
842 material in the two calculation methods considered. From the study carried out it was

843 possible to detect how the filling material has a significant effect on the stiffness of the  
844 support system in the convergence-confinement method and, therefore, on the load acting  
845 on the segmental lining. Instead, it has reduced and even negligible effects on the overall  
846 stiffness of the support system in the Einstein and Schwartz method used to carry out a  
847 first design of the segmental lining. With this latter calculation method, the analysis can  
848 proceed neglecting the presence of the filling material ring and directly obtaining the  
849 stresses affecting the segmental lining by adopting the stiffness parameters relating solely  
850 to segmental lining.

## 851 **Acknowledgment**

852 The authors wish to thank Master Builders Solutions for the permission granted to publish  
853 the results.

## 854 **Conflict of interests**

855 Authors declare they have no conflict of interest.

856

## 857 **References**

858 API Recommended Practice 13B-2 (2014). Recommended Practice for Field Testing Oil-  
859 Based Drilling Fluids. American Petroleum Institute.

860 Beghoul, M. and Demagh, R. (2019). Slurry shield tunneling in soft ground. Comparison  
861 between field data and 3D numerical simulation. *Studia Geotechnica et Mechanica*, 41(3),  
862 115–128.

863 Bezuijen, A. and Talmon, A. (2003) Processes around a TBM. *Geotechnical Aspects of*  
864 *Underground Construction in Soft Ground*, 48–56, 2008. doi:  
865 10.1201/9780203879986.ch1.

866 Casagrande, A. (1936). The determination of the pre-consolidation load and its practical  
867 significance. Proceedings of the international conference on soil mechanics and  
868 foundation engineering. 3. Harvard University Cambridge, 60–64.

869 Colombo, P., and Colleselli, F. (1996). *Elementi di Geotecnica*, Zanichelli, Bologna (in  
870 Italian).

871 Dai, Z., Bai, Y., Peng, F., and Liao, S. (2010). Study on mechanism of simultaneous  
872 backfilling grouting for shield tunnelling in soft soils. GeoShanghai Int. Conf. on Deep and  
873 Underground Excavations, ASCE, Reston, VA, 182–190.

874 Deutscher Ausschuss für unterirdisches Bauen e. V. (DAUB) (2013). Recommendations  
875 for the design, production and installation of segmental rings. Deutscher Ausschuss für  
876 unterirdisches Bauen e. V. (DAUB).

877 Dias, T.G.S. and Bezuijen, A. (2015). TBM Pressure Models - Observations, Theory and  
878 Practice. 15th Pan-American Conference on Soil Mechanics and Geotechnical  
879 Engineering - Geotechnical Synergy in Buenos Aires 2015, 347–374, 2015. doi:  
880 10.3233/978-1-61499-599-9-347.

881 DIN EN 480-4 (2006). Admixtures for concrete, mortar and grout - Test methods - Part 4:  
882 Determination of bleeding of concrete. Deutsche Institut für Normung e.V., Beuth Verlag,  
883 Berlin.

884 Do, N.-A., Dias, D., Oreste, P., Djeran-Maigre, I. (2014a). 2D Tunnel Numerical  
885 Investigation: The Influence of the Simplified Excavation Method on Tunnel Behaviour.  
886 Geotechnical and Geological Engineering, 32, 1, 43-58.

887 Do, N.A., Dias, D., Oreste, P., Djeran-Maigre, I. (2014b). 2D numerical investigations of  
888 twin tunnel interaction. Geomechanics and Engineering, 6(3), pp. 263-275.

889 Do, N.-A., Dias, D., Oreste, P., Djeran-Maigre, I. (2015). 2D numerical investigation of  
890 segmental tunnel lining under seismic loading. Soil Dynamics and Earthquake  
891 Engineering, 72, 66-76

892 Do, N.-A., Dias, D., Oreste, P. (2016). 3D numerical investigation of mechanized twin  
893 tunnels in soft ground - Influence of lagging distance between two tunnel faces.  
894 Engineering Structures 109, 117-125.

895 Einstein, H.H. and Schwartz, C.W. (1979). Simplified analysis for tunnel supports. J.  
896 Geotechnical Eng. Division ASCE, 105(4), 499-518.

897 Flores, A.Q. (2015). Physical and mechanical behavior of a two component cement-based  
898 grout for mechanized tunneling application. MSc Thesis, Universidade Federal do Rio de  
899 Janeiro, Brazil.

900 Guan Z., Deng T., Wang G. and Jiang Y. (2015). Studies on the key parameters in  
901 segmental lining design. Journal of Rock Mechanics and Geotechnical Engineering, 7,  
902 674-683.

903 Hashimoto, T., Brinkman, J., Konda, T., Kano, Y., and Feddema, A. (2004). Simultaneous  
904 backfill grouting, pressure development in construction phase and in the long-term.  
905 Underground space for sustainable urban development. Proceedings of the 30th ITA-  
906 AITES World Tunnel Congress, 19, 4–5, 447.

907 Hirata, T. (1989). Study on behavior of cohesive soil in type shield tunneling work and on  
908 construction technique. Doctoral Thesis, Kyoto University, Japan.

909 Janbu N. (1969) The resistance concept applied to deformations of soils. In: The 7<sup>th</sup>  
910 International Conference in Soil Mechanics and Foundation Engineering, Mexico, 191–  
911 196.

912 Hoek, E. (1994). Strength of rock and rock masses. ISRM News Journal, 2(2), 4-16.

913 Hoek, E., Kaiser, P.K. and Bawden, W.F. (1995). Support of underground excavations in  
914 hard rock. Rotterdam, Balkema.

915 Hoek, E. and Brown, E.T. (1997). Practical estimates of rock mass strength. Int. J. Rock  
916 Mech. & Mining Sci. & Geomechanics Abstracts, 34(8), 1165-1186.

917 Komiya, K., Soga, K., Akagi, H., Jafari, M.R. and Bolton, M.D. (2001). Soil consolidation  
918 associated with grouting during shield tunnelling in soft clayey ground. *Geotechnique*, 51,  
919 10, 835-846.

920 Lee, K. M., Rowe, R. K. and Lo, K.Y. (1992). Subsidence owing to tunneling. I. Estimating  
921 the gap parameter. *Canadian Geotechnical Journal*, 29, 929–940.

922 Maidl, B., Herrenknecht, M. and Anheuser, L. (1995). *Mechanised Shield Tunnelling*. Ernst  
923 & Sohn, Berlin.

924 Ochmański, M., Modoni, G. and Bzówka, J. (2018). Automated numerical modelling for the  
925 control of EPB technology. *Tunnelling and Underground Space Technology* 75, 117–128,  
926 <https://doi.org/10.1016/j.tust.2018.02.006>.

927 Ochmański, M., Modoni, G. and Spagnoli, G. (2020). Influence of the annulus grout on the  
928 soil-lining interaction for EBP tunneling. *Proc. of 10th International Symposium on*  
929 *Geotechnical Aspects of Underground Construction in Soft Ground* (in press).

930 Oh, J.Y. and Ziegler, M. (2014). Investigation on influence of tail void grouting on the  
931 surface settlements during shield tunneling using a stress-pore pressure coupled analysis.  
932 *KSCCE Journal of Civil Engineering*, 18(3), 803-811, DOI: [10.1007/s12205-014-1383-8](https://doi.org/10.1007/s12205-014-1383-8).

933 Oggeri C. and Ova G. (2004). Quality in tunnelling: ITA-AITES Working Group 16 Final  
934 report. *Tunnelling and Underground Space Technology* 19,(3) 239–227,  
935 doi:10.1016/j.tust.2004.01.002.

936 Oke, J., Vlachopoulos, N. and Diederichs, M. (2018). Improvement to the Convergence-  
937 Confinement Method: Inclusion of Support Installation Proximity and Stiffness. *Rock*  
938 *Mechanics and Rock Engineering*, 51, 1495–1519, [https://doi.org/10.1007/s00603-018-](https://doi.org/10.1007/s00603-018-1418-0)  
939 [1418-0](https://doi.org/10.1007/s00603-018-1418-0).

940 Oreste P. (2003). Analysis of structural interaction in tunnels using the convergence–  
941 confinement approach, *Tunnelling and Underground Space Technology*, Volume 18, Issue  
942 4, August 2003, Pages 347-363.

943 Oreste P. (2007). A numerical approach to the hyperstatic reaction method for the  
944 dimensioning of tunnel supports. *Tunn. Undergr. Sp. Tech.*, 22, 185–205.

945 Oreste P (2009) The convergence–confinement method: roles and limits in modern  
946 geomechanical tunnel design. *Am J Appl Sci* 6(4):757–771.

947 Oreste P (2015) Analysis of the Interaction between the Lining of a TBM Tunnel and the  
948 Ground Using the Convergence-Confinement Method. *American Journal of Applied*  
949 *Sciences* 12 (4), 276-283.

950 Oreste, P., Spagnoli, G., and Lo Bianco, L. (2016). A Combined Analytical and Numerical  
951 Approach for the Evaluation of Radial Loads on the Lining of Vertical Shafts. *Geotechnical*  
952 *and Geological Engineering* 34 (4), 1057-1065, [https://doi.org/10.1007/s10706-016-0026-](https://doi.org/10.1007/s10706-016-0026-6)  
953 [6](https://doi.org/10.1007/s10706-016-0026-6).

954 Oreste P., Spagnoli G., Luna Ramos A.C., and Seville L. (2018a). The Hyperstatic  
955 Reaction Method for the Analysis of the Sprayed Concrete Linings Behavior in Tunneling.  
956 *Geotech. Geol. Eng.*, 36(4), 2143–2169 <https://doi.org/10.1007/s10706-018-0454-6>.

957 Oreste P., Spagnoli G., and Luna Ramos A.C., (2018b). The Elastic Modulus Variation  
958 During the Shotcrete Curing Jointly Investigated by the Convergence-Confinement and the  
959 Hyperstatic Reaction Methods. *Geotech. Geol. Eng.*, [https://doi.org/10.1007/s10706-018-](https://doi.org/10.1007/s10706-018-0698-1)  
960 [0698-1](https://doi.org/10.1007/s10706-018-0698-1).

961 Oreste P., Spagnoli G., Luna Ramos A.C., and Hedayat, A. (2019) Assessment of the  
962 Safety Factor Evolution of the Shotcrete Lining for Different Curing Ages. *Geotechnical*  
963 *and Geological Engineering* 37 (6), 5555-5563, [https://doi.org/10.1007/s10706-019-00990-](https://doi.org/10.1007/s10706-019-00990-2)  
964 [2](https://doi.org/10.1007/s10706-019-00990-2).

965 Park, H., Oh, J.Y., Kim, D., and Chang S. (2018). Monitoring and analysis of ground  
966 settlement induced by tunnelling with slurry pressure-balanced Tunnel Boring Machine.  
967 *Advances in Civil Engineering*, 2018, ID 5879402, <https://doi.org/10.1155/2018/5879402>.

968 Pelizza, S., Peila, D., Sorge, R., Cignitti, F. (2011). Back-fill grout with two component mix  
969 in EPB tunneling to minimize surface settlements: Rome Metro - Line C case history.  
970 Proceedings of Geotechnical Aspects of Underground Construction in Soft Ground,  
971 Viggiani, G. (ed.), 291-299, Taylor & Francis Group, London.

972 Pelizza, S., Oreste, P.P., Peila, D., Oggeri, C. (2000), Stability analysis of a large cavern in  
973 Italy for quarrying exploitation of a pink marble. Tunnelling and Underground Space  
974 Technology 15(4), pp. 421-435.

975 Serafim, J. L., and Pereira, J. P. (1983). Constructions of the geomechanics classification  
976 of Bieniawski. In Proc. Int. Symp. on Engg. Geol. and Underground Construction. LNEC,  
977 Lisob, Portugal.

978 Shah, R., Lavasan, A.A., Peila, D., Todaro, C., Luciani, A. and Schanz, T. (2018).  
979 Numerical study on backfilling the tail void using a two-component grout. J. Mater. Civ.  
980 Eng., 30(3): 04018003.

981 Spagnoli, G., Oreste, P., and Lo Bianco L. (2016). New Equations for Estimating Radial  
982 Loads on Deep Shaft Linings in Weak Rocks. International Journal of Geomechanics 16  
983 (6), 06016006, [https://doi.org/10.1061/\(ASCE\)GM.1943-5622.0000657](https://doi.org/10.1061/(ASCE)GM.1943-5622.0000657).

984 Spagnoli, G., Oreste, P., and Lo Bianco L. (2017). Estimation of Shaft Radial  
985 Displacement beyond the Excavation Bottom before Installation of Permanent Lining in  
986 Nondilatant Weak Rocks with a Novel Formulation. International Journal of Geomechanics  
987 17 (9), 04017051, [https://doi.org/10.1061/\(ASCE\)GM.1943-5622.0000949](https://doi.org/10.1061/(ASCE)GM.1943-5622.0000949).

988 Talmon, A.M. and Bezuijen, A. (2005). Grouting the tail void of bored tunnels: the role of  
989 hardening and consolidation of grouts. Proceedings of the 5th International Symposium TC  
990 28 - Geotechnical Aspects of Underground Construction in Soft Ground, 125-130,  
991 Balkema, Rotterdam.

992 Thewes, M. and Budach, C. (2009). Grouting of the annular gap in shield tunnelling-An  
993 important factor for minimisation of settlements and production performance. Proceedings

994 of the ITA-AITES World Tunnel Congress 2009 “Safe Tunnelling for the City and  
995 Environment”, pp. 1–9.

996 Todaro, C., Peila, L., Luciani, A., Carigi, A., Martinelli, D. and Boscaro, A. (2019). Two  
997 component backfilling in shield tunneling: laboratory procedure and results of a test  
998 campaign. In Proceedings of the WTC 2019 ITA-AITES World Tunnel Congress (WTC  
999 2019), May 3-9, 2019, Naples, Italy, Peila, D., Viggiani, G. and Celestino, T. (eds), CRC  
1000 Press, Boca Raton.

1001 Vu, M.N., Broere, W. and Bosch, J. (2016). Volume loss in shallow tunnelling. *Tunnelling  
1002 and Underground Space*, 59, 77-90, doi: 10.1016/j.tust.2016.06.011.